



Article

Intestinal Epithelium-Derived Luminally Released Extracellular Vesicles in Sepsis Exhibit the Ability to Suppress TNF- α and IL-17A Expression in Mucosal Inflammation

Michael G. Appiah ^{1,†}, Eun Jeong Park ^{1,*},, Samuel Darkwah ¹, Eiji Kawamoto ^{1,2}, Yuichi Akama ^{1,2},, Arong Gaowa ¹, Manisha Kalsan ³,, Shandar Ahmad ³ and Motomu Shimaoka ^{1,*}

¹ Department of Molecular Pathobiology and Cell Adhesion Biology, Mie University Graduate School of Medicine, Tsu, Mie 514-8507, Japan; 317DS06@m.mie-u.ac.jp (M.G.A.); 316DS12@m.mie-u.ac.jp (S.D.); a_2.uk@mac.com (E.K.); y-akama@clin.medic.mie-u.ac.jp (Y.A.); arong-g@doc.medic.mie-u.ac.jp (A.G.)

² Department of Emergency and Critical Care Center, Mie University Hospital, Tsu, Mie 514-8507, Japan

³ School of Computational and Integrative Sciences, Jawaharlal Nehru University, New Delhi 110067, India; manisha8013@gmail.com (M.K.); shandar@jnu.ac.in (S.A.)

* Correspondence: epark@doc.medic.mie-u.ac.jp (E.J.P.); shimaoka@doc.medic.mie-u.ac.jp (M.S.)

† Contributed equally and share first authorship.

Received: 6 October 2020; Accepted: 9 November 2020; Published: 10 November 2020



Abstract: Sepsis is a systemic inflammatory disorder induced by a dysregulated immune response to infection resulting in dysfunction of multiple critical organs, including the intestines. Previous studies have reported contrasting results regarding the abilities of exosomes circulating in the blood of sepsis mice and patients to either promote or suppress inflammation. Little is known about how the gut epithelial cell-derived exosomes released in the intestinal luminal space during sepsis affect mucosal inflammation. To study this question, we isolated extracellular vesicles (EVs) from intestinal lavage of septic mice. The EVs expressed typical exosomal (CD63 and CD9) and epithelial (EpCAM) markers, which were further increased by sepsis. Moreover, septic-EV injection into inflamed gut induced a significant reduction in the messaging of pro-inflammatory cytokines TNF- α and IL-17A. MicroRNA (miRNA) profiling and reverse transcription and quantitative polymerase chain reaction (RT-qPCR) revealed a sepsis-induced exosomal increase in multiple miRNAs, which putatively target TNF- α and IL-17A. These results imply that intestinal epithelial cell (IEC)-derived luminal EVs carry miRNAs that mitigate pro-inflammatory responses. Taken together, our study proposes a novel mechanism by which IEC EVs released during sepsis transfer regulatory miRNAs to cells, possibly contributing to the amelioration of gut inflammation.

Keywords: sepsis; intestinal epithelial cells; inflammation; extracellular vesicles; TNF- α ; IL-17A; miRNAs

1. Introduction

Sepsis is a life-threatening organ dysfunction resulting from a dysregulated host immune response to infection [1]. Sepsis is a principal cause of mortality in the intensive care unit (ICU) setting, with an estimated 48.9 million case incidence and 11 million deaths occurring globally in 2017 [2]. The major causes of mortality and morbidity stem from multiple organ failure. The gut is one of the major organs damaged during sepsis. Gut epithelial-barrier dysfunction is a primary pathological feature in sepsis and has been shown to be detrimental to survival [3]. In sepsis, splanchnic hypoperfusion causes gut

injury, which in turn results in the release of gut-derived pro-inflammatory factors [4,5] that reach the systemic circulation through the mesenteric lymph [6–9]; a process thought to exacerbate and maintain an inflammatory response that culminates in multiple organ failure [10]. Thus, the gut has been described as the “motor” of multiple organ dysfunction syndrome (MODS) both in sepsis and other critical illnesses, due to its potential role as a portal for generating systemic immune responses [11]. Infectious and inflammatory injury to the intestinal epithelial cells not only compromises barrier functionality, but also induces the secretion of pro-inflammatory and regulatory cytokines [12–14]. Pro-inflammatory cytokines secreted into the intestinal luminal space during sepsis are thought to act as important regional mediators that complicate the pathology of intestinal failure [14]. As detailed in the following sections, we have explored the role of extracellular vesicles (EVs) as an alternative/additive regional mediator to lumenally secreted cytokines in sepsis.

Small EVs called exosomes are biologically functional nanoparticles released from virtually all cells including intestinal epithelial cells [15]. EVs serve as mediators of intercellular communication between both neighboring and distant cells. EVs carry and directionally transfer a repertoire of bioactive molecules, such as proteins, lipids, and genetic materials (e.g., mRNA, miRNA), all of which are capable of modifying the functions of the recipient cells [16]. EVs secreted from immune cells, platelets, and endothelial cells have been shown to play important roles in the pathogenesis of sepsis. Dendritic cells have been shown to produce EVs that abrogate septic inflammatory responses by delivering milk fat globule EGF factor VIII (MFG-E8) [17]. EVs derived from circulating platelets have been reported to aggravate multiple organ dysfunction during sepsis by transferring reactive oxygen species and pro-inflammatory miRNAs to their target cells [18]. Endothelial exosomes in septic mice have been shown to exert their protective effects against cardiomyopathy by delivering heat shock protein [19]. In addition, exosomes in the plasma of septic patients, which are likely to be derived from multiple cells such as leukocytes, platelets, and vascular endothelial cells, have been shown not only to contain miRNAs related to inflammation and cell-cycle regulation [20], but also to express the programmed cell death 1 (PD-1) ligand [21].

IECs have been shown to secrete EVs in two alternative directions, basolaterally and apically. Chen et al. have shown that basolaterally released IEC EVs carry food antigens while expressing $\alpha V\beta 6$ integrin that activates TGF- β thereby inducing the tolerogenic capacities of dendritic cells in the lamina propria space [22]. Kojima et al. have shown in a rat model of trauma and hemorrhagic shock that basolaterally released IEC EVs, with upregulated apoptosis-inducing Fas ligand expression, were drained to the mesenteric lymph nodes, thereby inhibiting the functions of dendritic cells and lymphocytes [23]. By contrast, using an IEC line infected by a protozoan parasite, Hu et al. have shown that exosomes released from IECs to the apical side carry antimicrobial peptides, thereby playing a role in host defense [24]. Deng et al. have shown in vivo that apically released IEC EVs isolated from the intraluminal space of the mouse intestine carry prostaglandin E2 to suppress natural killer T-cell functions [25]. In addition, using colonic fluid aspirates from inflammatory bowel disease patients, Mitsuhashi et al. have shown that apically released IEC in the intraluminal space become enriched with pro-inflammatory cytokines [26].

These previous reports point to the potential regulatory roles of IEC-released EVs; however, their nature and immuno-modulatory effects in sepsis remain to be elucidated. Here, we have studied the IEC-derived EVs released into the intestinal luminal space, demonstrating their actions to suppress TNF- α and IL-17A expression in intestinal mucosal inflammation in vivo. Lumenally-released IEC EVs in sepsis are thought to act in a para- and autocrine manner to counter-balance inflammation and, thus, contribute to the maintenance of regional immune-homeostasis.

2. Results

2.1. Luminal Lavage EVs Are Epithelial Derived and Express Exosome Markers

Using differential ultracentrifugation, EVs were isolated from the intestinal lavage fluids of septic mice 24 h after CLP induction in mice. As a control, EVs were isolated from the intestinal lavage fluids of sham-operated (laparotomy) mice 24 h after the procedure. By this time septic mice manifested shock symptoms such as lethargy, piloerection, periorbital exudate, and diarrhea [27] and by 72 h were all dead (Supplementary Materials Figure S1). Compared to those of control mice, mRNA levels of the IL-6, IL-10, and CCL3 in peripheral blood mononuclear cells (PBMCs) of septic mice were significantly increased (Figure S2), all of which are known to be key markers of sepsis severity and mortality [28,29].

EVs isolated from large intestine lavage fluid expressed the epithelial marker EpCAM, but not the leukocyte marker CD45 or the platelet maker CD41 (Figure 1A). Thus, the majority of EVs were derived from gut epithelial cells, while only a small proportion was presumably from the circulation. EVs isolated from the large intestine lavage fluid showed the typical exosomal markers CD63 and CD9 (Figure 1A). In contrast, EVs from the small intestine lavage fluid showed only CD63 but lacked CD9 and EpCAM-1 expression (Figure S3). In some experiments, EVs isolated via the more stringent C-DGUC method showed similar results (Figure S4). Therefore, EVs from the large intestine were classified as belonging to the typical exosome category while those from the small intestine were excluded. For the sake of simplicity and clarity, in the sections that follow we focus on the EVs from the large intestine lavage fluid, although we are aware that some of these EVs isolated may have been secreted from the small intestine.

Expression of the tetraspanins CD63 and CD9 from large intestine lavage EVs was upregulated during sepsis (Figure 1A). Moreover, EpCAM-1 on those EVs was also enhanced by sepsis (Figure 1A). Thus, sepsis-induced upregulation of typical exosomal and epithelial marker expressions may reflect the possibility that luminal release of IEC-derived EVs is facilitated by the pathological condition of sepsis.

The sizes and particle densities of the EVs were measured using nanoparticle tracking analysis (NTA) or dynamic light scattering (DLS). The EVs were found to range from 50 to 600 nm and displayed a major peak at approximately 200 nm (Figure 1B). The density of EVs from sepsis mice was $1.10 \pm 0.16 \times 10^9$ while that from sham-treated mice was $0.82 \pm 0.17 \times 10^9$ particles per mL (Figure 1C). The average sizes of the EVs were 157 ± 17 nm and 208 ± 26 nm for sepsis and control mice, respectively (Figure 1D).

As gut lumen harbors numerous microflora [30], the EVs might contain bacterial EVs. Thus, we sought to measure the level of bacteria endotoxin (lipopolysaccharide; LPS) that is contained in the EVs secreted from gram-negative bacteria. Measurements by ELISA revealed that LPS levels in all EV samples from the luminal lavage of mice and from the fecal samples of septic patients were similar to those of a negative control (BSA), and much lower than those in the plasma and feces of septic mice (Figure S5). Notably, the plasma samples of septic mice showed increased LPS levels. Therefore, LPS levels were barely detectable in the EV samples. Although it is still possible that trace amount of bacterial and/or fungal components were present, IEC-derived exosomes constituted the majority of the EV samples isolated from the large intestinal lavage fluids in this study.

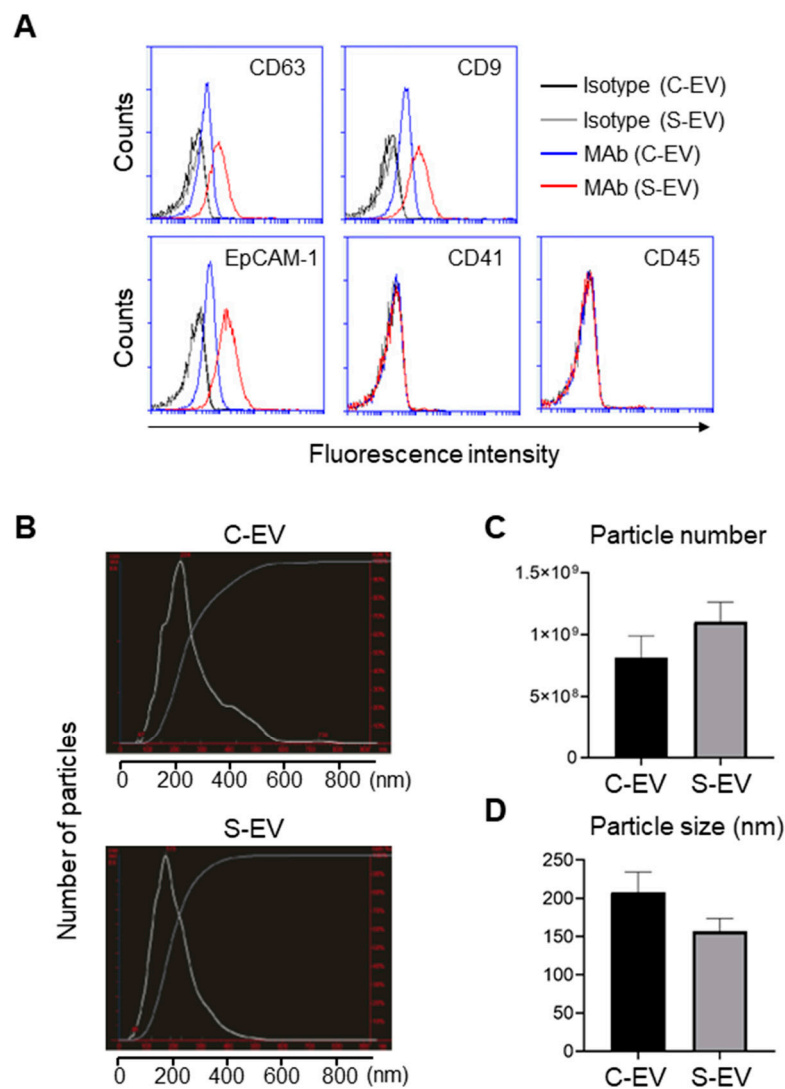


Figure 1. Characterization of EVs isolated from luminal washes in large intestines of control and septic mice. **(A)** Flow cytometry analysis of EVs isolated from luminal washes in large intestines of control and septic mice. EVs were isolated by differential UC and adsorbed on 4 μm poly-L-lysine microbeads overnight. Immobilized EVs (20 μg) were stained with indicated monoclonal antibodies (MAb) and subjected to flow cytometry to evaluate their expression. Representative histograms show changes in expression of indicated marker. Black line, isotype (C-EV); gray line, isotype (S-EV); blue line, MAb (C-EV); and red line, MAb (S-EV). **(B)** Representative NanoSight LM10 images showing sizes of EVs from control (top) and septic (down) mice. **(C)** Particle number of EVs as quantified by NTA. **(D)** Size distribution of gut-derived C-EVs ($N = 15$) and S-EVs ($N = 16$) mice groups as measured by dynamic light scattering (DLS) device. C-EV, control extracellular vesicle; and S-EV, sepsis extracellular vesicle.

2.2. Luminal Lavage EVs of Sepsis Mice Regulate Pro-Inflammatory Cytokine Expression in a Colitis Model

To test our research hypothesis that intestinal epithelial EVs function as a para- and autocrine regulator of mucosal immunopathology, we first performed ileal-loop assay in which lumenally secreted intestinal epithelial EVs were injected into the luminal space of the tied ileum of healthy mice, and in a separate experiment, the tied ileum of DSS-induced colitis mice. Although DSS-induced colitis is not directly relevant to sepsis-induced mucosal immunopathology, we reasoned that mucosal inflammation in DSS-induced colitis could serve as an *in vivo* bioassay for studying the ability of lumenally-secreted intestinal epithelial EVs to modulate regional immunological responses. Mucosal inflammation was

induced by the oral administration of 2.5% DSS-containing drinking water for seven days. This in vivo bioassay system could recapitulate a scenario in which lumenally secreted intestinal epithelial EVs act on mucosal inflammation. Eighteen hours after EV treatment, the mice were sacrificed and the intestinal tissues were harvested and subjected to quantitative RT-PCR analysis of some key pro-inflammatory mediators in both septic [28,31] and DSS-induced mucosal inflammation [32,33].

In the ileal tissues of healthy mice, sepsis EVs (S-EVs) downregulated messages of the pro-inflammatory cytokines including TNF- α , IL-1 β , IL-6, IL-17A, and IL-22 (Figure S6). DSS-treatment increased the expressions of all the aforementioned cytokines in the gut tissues, as was evident in vehicle (PBS)-administered mice (Figure 2 and Figure S7). We noted that, administration of S-EVs into the ileal loop of DSS-colitis mice significantly suppressed the mucosal inflammation-associated increase in TNF- α and IL-17A compared to that of control EVs (C-EVs) (Figure 2). Contrasting effects were, however, seen between both EVs with regards to IL-1 β , IL-6, and IL-22 as their expressions were significantly decreased by S-EVs but increased by C-EVs (Figure S7). We compared these results with those which were isolated by using the cushioned-density gradient ultracentrifugation (C-DGUC) which is another method offering improved purity to EVs [34,35], in order to validate biological effects of the EV samples isolated by using differential UC. As a result, treatment with S-EVs isolated by C-DGUC was also shown to reverse the upregulation of TNF- α and IL-17A in the DSS-induced gut inflammation (Figure S8), suggesting that S-EVs may possess a healing effect in the inflamed intestinal tissues.

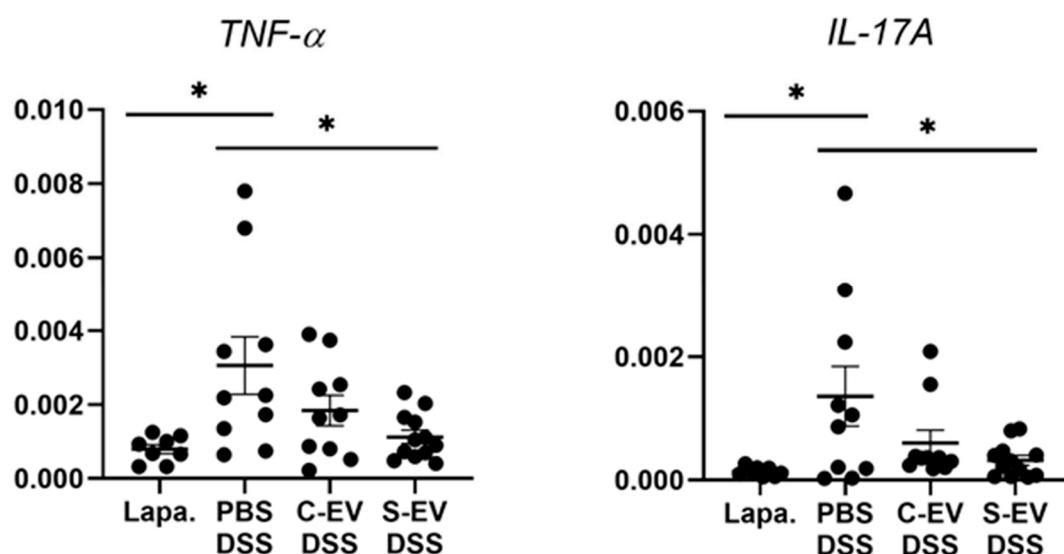


Figure 2. RT-qPCR analysis for gene expression of TNF- α and IL-17A. Gut inflammation was induced in the mice by 2.5% DSS-containing drinking water for seven days. Direct injection of either vehicle or differential UC-isolated EVs into the lumen of the tied ileum was done on day 7 and the tissues were separated after 18 h for RNA extraction. Relative expression of genes to β -actin in ileal-loop tissues of mice was accessed. Lapa, laparotomy; PBS, phosphate-buffered saline (200 μ L); C-EV, control EVs (50 μ g/200 μ L) injected; S-EV, sepsis EVs (50 μ g/200 μ L) injected into ileal space; and DSS, dextran sulfate sodium. Other abbreviations: TNF- α , tumor necrosis factor- α ; IL-17A, interleukin-17A. $N = 8$ –12. * $p < 0.05$.

We next sought to confirm, using in vitro system, the regulatory effects of S-EVs on gut expression of pro-inflammatory mediators. Based on our hypothesis that gut epithelium is the main target affected by S-EVs, we isolated primary gut ECs, confirmed their expression of EpCAM (Figure S9A), and then treated with different EV doses (1, 5, or 10 μ g/mL) to determine the impacts on regulating TNF- α and IL-17A expression. But, S-EVs as well as C-EVs didn't exhibit any significant reduction, at any EV concentration used, in TNF- α and IL-17A expression of primary gut ECs, when compared with vehicle

treatment (Figure S9B). Accordingly, establishment of more physiologically relevant models might be beneficial to achieve in vitro outcome that correlates with in vivo result. We have discussed more about this matter in Section 3 below.

2.3. Luminal Lavage EVs in Sepsis Enrich the miRNAs Regulating Inflammation

Here, we investigated the ability of intestinal epithelial EVs in sepsis to suppress TNF- α , and IL-17A based on the assumption that such a capability would primarily be mediated by exosomal miRNAs. To this end, we conducted in silico analysis of exosomal miRNAs. To compare miRNA profiles of the intestinal epithelial EVs in septic mice versus those of control mice, we performed small-RNA deep sequencing, identifying a total of 417 miRNAs based on criteria stipulating a value of ≥ 1 reads per kilobase of transcript per million mapped reads (RPKM) (Table S2). Of the 417 miRNAs, 45 and 190 miRNAs were expressed exclusively in control (C-EVs) and sepsis EVs (S-EVs), respectively, while 182 miRNAs were expressed in both (Figure 3A). Moreover, 292 miRNAs were upregulated, whereas 68 miRNAs were downregulated in S-EVs with a fold change of ≥ 2 compared to control EVs (Figure 3B). Gene ontology (GO) enrichment analysis of targets of the sepsis-increased miRNAs revealed transcription regulation-related GO molecular functions. This was corroborated by the enriched transcription-related GO biological process terms (Figure S10A and data not shown). In addition, GO cellular compartments were enriched with nucleus-related terms (Figure S10B).

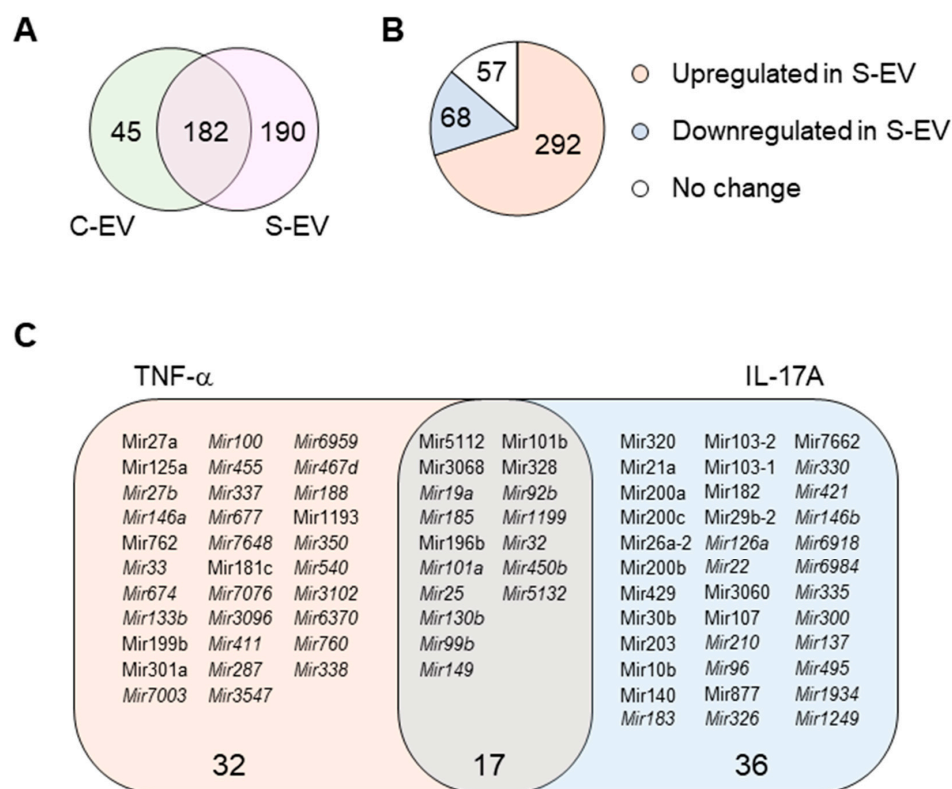


Figure 3. miRNA profiling of gut luminal EVs. (A) Venn diagram of microRNA distribution in control and septic gut luminal EVs. (B) Pie chart of differential expression of gut luminal EV microRNAs based on fold-change (S-EV/C-EV) in miRNA RPKM values. (C) TNF- α - and IL-17A-targeting miRNAs among all the sepsis-upregulated miRNAs. The miRNAs upregulated during sepsis indicate those which showed more than a two-fold increase in RPKM values in S-EV compared with C-EV. All miRNAs were chosen based on a criteria of >1 RPKM value. The miRNAs detected only in S-EVs are in italic. S-EV, sepsis EVs; and C-EV, control EVs.

Using a TargetScan bioinformatics analysis that concentrated on miRNAs upregulated in the intestinal epithelial EVs during sepsis, we examined those miRNAs predicted to target TNF- α , and IL-17A. We found 32 and 36 miRNAs that targeted TNF- α and IL-17A, respectively, as well as 17 others which target both genes (Figure 3C and Table S3). We selected some of the TNF- α and IL-17A targeting miRNAs based on knowledge of their involvement in modulating inflammatory response (Figure 4A) and using RT-qPCR, we confirmed upregulation of these miRNAs in sepsis intestinal epithelial EVs, compared with control intestinal epithelial EVs (Figure 4B).

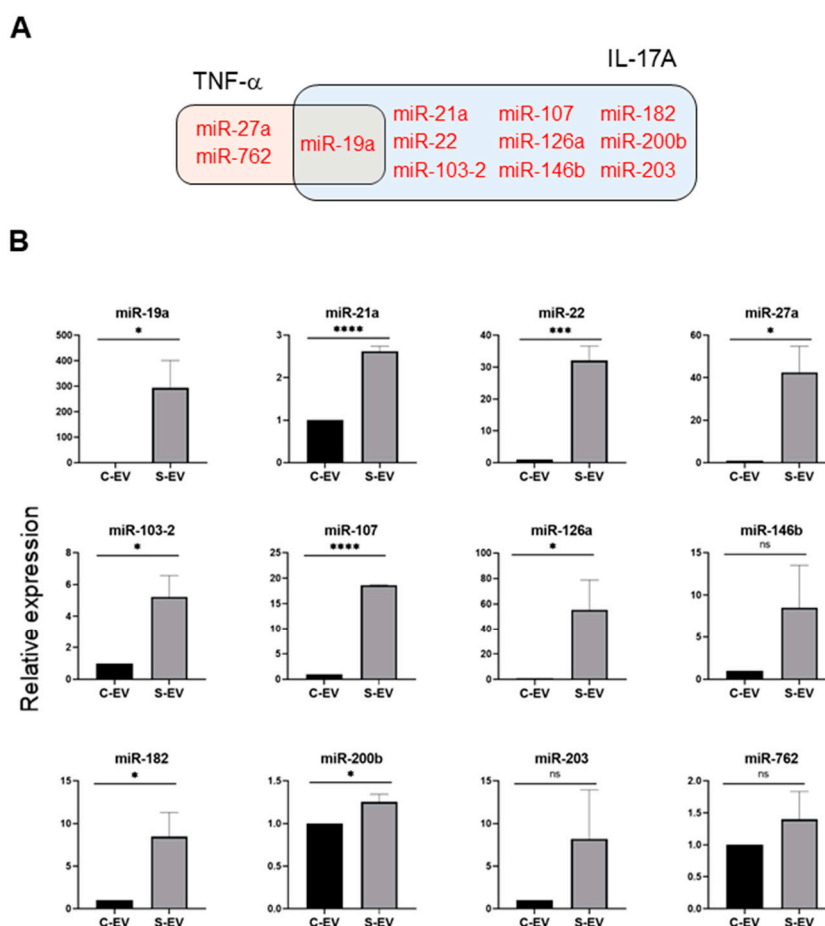


Figure 4. Sepsis EVs (S-EVs) enrich 12 chosen miRNAs expected to target *TNF- α* and *IL-17A*. (A) Among sepsis-augmented miRNAs in S-EVs, 12 miRNAs shown in Venn diagram were selected to further analyze their expressions. (B) RT-qPCR analysis for miRNA expressions in the EVs. These miRNAs were tested for their increased enrichment in S-EV. As a control, U6 was used to normalize miRNA levels. Total RNAs were isolated from EVs pooled from 5 mice in each group. At least four separate experiments were performed. Results are shown as the mean \pm SEM. S-EV, sepsis EVs; and C-EV, control EVs. * $p < 0.05$; *** $p < 0.001$; **** $p < 0.0001$; and ns, not significant.

3. Discussion

Accumulating evidence suggests that extracellular vesicles (EVs) are involved in the pathogenesis of sepsis, with different effects based on the multiple sources and targets of EVs [36,37]. Much less is known, however, about how EVs are shed from the gut and their precise roles in this compartment, which perpetuates septic inflammatory responses. Thus, we investigated intestinal epithelial cell (IEC)-derived EVs in sepsis and their roles in inflammation. IECs secrete various cytokines and chemokines, especially under inflammatory conditions [38]. The recognition of pathogen-associated molecular patterns (PAMPs) by pattern recognition receptors (PRRs) on IECs and other cells of the

mucosal immune system during sepsis stimulates the release of a plethora of pro-inflammatory cytokines, which in turn induces the infiltration of leukocytes to the gut mucosa, further exacerbating the inflammatory response [39]. This dysregulated inflammatory response may lead to vasodilatation, increased capillary leakage, and decreased oxygen supply to the intestinal epithelium, which can cause a breakdown of the epithelial barrier and foster translocation of gut bacteria and/or their products into previously sterile sites [40]. In the current study, we found that EVs from the intestinal lumen of septic mice exhibited significant changes compared to their healthy counterparts. In addition, there appeared to be a slight increase in the number of EVs during sepsis (Figure 1C). These results are consistent, at least in part, with those of a previous report that showed increased numbers of EVs in the plasma of septic mice [18].

Although the roles played by exosomes in the pathogenesis of sepsis have been studied for years, controversy persists regarding whether exosomes exert harmful or protective roles. Some previous studies found that exosomes isolated from septic mice and patients have harmful effects [41–44]. For example, exosomes derived from the platelets of septic patients exhibited a negative inotropic effect on an isolated rabbit heart, which may be evidence of a possible link to sepsis-induced myocardial dysfunction [41]. Exosomes from septic mice suppressed the contraction of the left ventricle of the heart in healthy recipient mice [43]. Exosomes from mice suffering a septic acute lung injury induced lung inflammation in healthy recipient mice, possibly through exosomal miR-155 [44]. In addition, treatment with small molecule GW4869 that has been posited to inhibit exosome biogenesis and release, dampened sepsis-induced cardiac inflammation and dysfunction, leading to the improved survival rates in CLP-induced septic mice [42]. In contrast, other studies demonstrated that exosomes isolated from septic mice and patients exhibited protective effects [45,46]. For instance, exosomes isolated from the plasma of septic patients improved survival rates in a feces-induced sepsis mouse model, possibly via miR-7-5p which inhibits T-lymphocyte apoptosis [46]. Exosomes from septic mice alleviated the progression of lung and liver injury, thereby improving the survival rates of CLP-induced septic mice [45]. The results presented in this study have shown that lumenally secreted intestinal epithelial exosomes suppresses TNF- α and IL-17A expression in inflamed mucosal tissues. Thus, our study supports the hypothesis that sepsis induces intestinal epithelial cells to secrete exosomes in order to dampen local mucosal inflammation.

The suppression of tissue TNF- α and IL-17A expression by septic luminal epithelial exosomes is thought to be mediated by exosomal miRNAs targeting the 3'-UTR of TNF- α and IL-17A mRNAs. Indeed, IECs are known to produce both TNF- α and IL-17A, which are critical players in the pathogenesis of sepsis [47,48] although other sources of TNF- α (macrophages, fibroblasts) and IL-17A ($\gamma\delta$ T cells, ILC3) exist especially in the inflamed gut mucosa. In particular, Paneth cell-derived IL-17A has been shown to help induce systemic inflammatory responses in a model of TNF-induced shock [48]. IEC-derived exosomes released into mesenteric lymph following trauma and hemorrhagic shock were reported to possess an ability to induce acute lung injury [49]. Recently, IEC-derived exosomes were shown to induce the inflammatory responses of splenocytes in a parasite-infection model [50]. Intriguingly, in the same model but examining parasite infection with *Cryptosporidium parvum*, apically released IEC exosomes exhibited microbicidal activity against *C. parvum* [24].

The constitution of gut microbiome is altered by sepsis, which may contribute to organ dysfunction [51,52]. S-EVs are thought to be capable of eliciting inflammation by delivering cytokines or damage-associated molecular pattern to target tissues [53]. In accordance with these notions one can consider that the EVs secreted during sepsis may reshape contents of gut microbiota by direct or indirect transfer of their biologically active contents including pro-inflammatory mediators or miRNAs. In current study, IEC-derived EVs of septic mice have been proposed to play a regulatory, but not degenerating, role. Consequently, it is worthwhile to test if the EVs derived from different sources (e.g., IECs, macrophages, lymphocytes, or blood) during sepsis influence the composition of the gut microbiome [54]. Indeed, elaborate acquisition of information on relationship between

S-EV-induced microbiome alteration and pathophysiologic outcome will be instrumental to design EV-based therapeutics to gut inflammation in the future.

To elicit miRNA-mediated gene silencing, exosomes administered into the intraluminal space are likely to be uptaken by those cells in the gut mucosa, recapitulating the para- and autocrine mechanisms that maintain local immune homeostasis in gut mucosal tissues. The luminal spaces of the large and small intestines contain EVs secreted not only from gut epithelial cells, but also from commensal bacteria and other microorganisms. Bacterial EVs from mice have been shown to elicit systemic inflammatory responses through Toll-like receptors 2 and 4 when intraperitoneally injected [55]. Although we have excluded the major contamination of bacterial components by measuring the endotoxin levels of our EV samples, we are aware that a trace amount of LPS and/or other microbial components might be present. For this reason, we avoided administering them intravenously in vivo. Instead, we selected the ileal-loop assay to test the roles played by the EV samples in the gut microenvironments that commensal bacteria co-habit. Interestingly, it has been shown that some of the intestinal epithelial cell-derived miRNAs do enter commensal bacteria, thereby regulating bacterial gene expression and affecting bacterial growth [56]. Thus, in addition to host cells in the gut, commensal bacteria might alternatively be subjected to EV-mediated regulation in order to maintain mucosal immune homeostasis.

We found that 292 miRNAs were upregulated in IEC-derived EVs with sepsis, an amount similar to those reported in previous studies that utilized septic clinical and mouse EVs [18,20]. The GO results from the clinical EV samples predicted miRNA profiling for inflammatory and immune responses [20]. In our GO analysis, the transcription-related molecular functions and biological processes were upregulated for enriched miRNAs (Figure S10A). This disparity could have occurred, at least partly, due to differences in the experimental subjects, exosome isolation method, timeline analyses, and/or the tissues from which the exosomes were isolated.

Following the observation that S-EVs downregulate messaging of TNF- α and IL-17A in the inflamed gut, we attempted to confirm the sepsis-increased expression of several miRNAs predicted to target these genes. We realized that multiple miRNAs in luminal EVs, including miR-19a, -21, -27a, -126, 146b, and -200b were upregulated by sepsis (Figure 4). Previous reports support the possible roles of those EV miRNAs in mitigating systemic inflammatory responses. Overexpression of miR-19a reduced TNF- α in a model of LPS-induced endometritis [57]. Paclitaxel-induced amelioration of liver injury in sepsis was empowered by miR-27a-mediated downregulation of inflammatory responses [58], whereas increased miR-27a during sepsis aggravated the inflammatory response [59], demonstrating that the exact role played by this miRNA in modulating sepsis pathogenesis remains incompletely understood. In an ischemic preconditioning-polymicrobial sepsis model, exosomal miR-21 repressed NF- κ B signaling and decreased pro-inflammatory cytokine production in remote organs leading to increased survival in septic mice [60]. miR-126 carried by endothelial progenitor cell exosomes protected against sepsis-induced microvascular dysfunction, lung and kidney injury, and cardiomyopathy [19,61,62]. miR-146b ameliorates LPS-induced acute lung injury [63], whereas its reduction increases IL-17A and promotes T cell acute lymphoblastic leukemia cell migration and invasion [64]. Transfection of HEK293 and THP-1 cells stably expressing TLR4 with miR-200b, and miR-200c mitigates activation of NF- κ B activation and diminishes endotoxin-induced expression of TNF- α , IL-6, and other pro-inflammatory cytokines [65]. Considering all these evidence, our study supports the contention that sepsis-enhanced functional miRNAs in IEC EVs possess the ability to regulate TNF- α and IL-17A expression in the gut. However, our study lacks a functional examination of treating inhibitors for specific miRNAs in order to confirm the effects of EVs. Thus, it would be worthwhile to conduct an antagonizing and/or mimicking assay in vivo in the context of inflammations.

IL-6, IL-22, and IL-1 β were significantly upregulated by C-EV compared to PBS and/or S-EV (Figure S7). Though known for their pro-inflammatory functions, IL-6 and IL-22 protect IECs from apoptosis and stimulate IEC proliferation and wound repair [66–68]. Thus, the definitive effect of the luminal IEC-derived EV-induced cytokine modulation on the restitution and integrity of the gut epithelial barrier under inflammatory conditions remains to be elucidated.

As aforementioned, S-EVs were not able to reduce TNF- α and IL-17A expression in the culture of isolated IECs (Figure S9). A few possible explanations for this discrepancy can be regarded. First, our *in vivo* data (Figure 2) indicate that S-EVs exert a regulatory effect on expression of TNF- α and IL-17A in the condition of gut inflammation. Thus, it will be worthy to verify these regulatory effects of S-EVs in gut ECs of the inflamed intestines. Second, because a majority of the isolated cells proved to be epithelial positive, it is unlikely that other immune cells such as macrophages or lymphocytes affect the outcome. Thus, one cannot rule out the possibility that any of those immune cells are sensitive to EV-mediated downregulation of expression of both mediators in immune cells. Third, it is imperative to exploit physiologically relevant condition of gut epithelia. Therefore, culturing intestinal organoids might be suitable for examination, in near future, to corroborate the regulatory effects of S-EVs, which was observed in our *in vivo* study.

In conclusion, we have shown that gut-lavage EVs are exclusively IEC-derived and that their expression of an epithelial marker (EpCAM) is augmented by sepsis. Sepsis EVs, compared to controls, were capable of downregulating pro-inflammatory gene expression in a gut-inflamed model. The IEC-derived EVs transformed, acquiring a highly regulatory miRNA composition following sepsis, thereby suggesting their potential role in modulating gut inflammation. This process is illustrated in Figure 5, in which septic IEC-derived luminal EVs regulate mucosal inflammatory response in the gut. Taken together, our study could provide potential clues to the previously unappreciated role played by sepsis EVs in the inflamed gut.

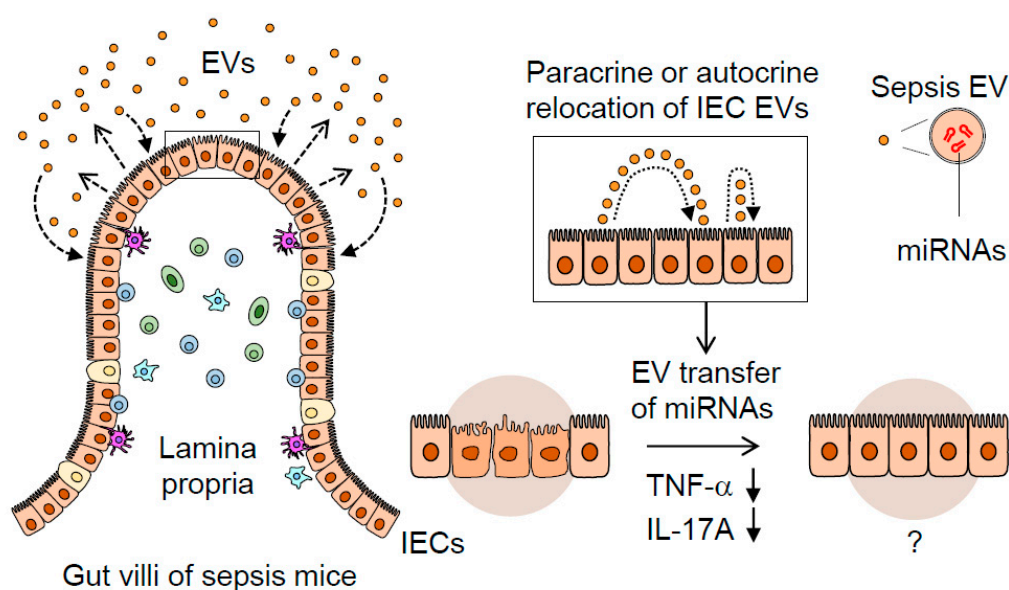


Figure 5. A proposed mechanism illustrating the dynamic role of septic IEC-derived luminal EVs in regulating gut inflammation. Sepsis induces gut-barrier dysfunction and epithelial injury. Sepsis-induced luminal release of EVs increases their epithelial trait. The luminal EVs possessing different miRNA expression levels relocate themselves to IECs in either a paracrine or autocrine fashion. Thus, the EVs secreted from IECs are thought to contribute to dampening pro-inflammatory responses in sepsis-damaged gut mucosa via the transfer of regulatory miRNAs.

4. Materials and Methods

4.1. Mice

Balb/c mice (8–12 weeks old) were obtained from Japan SLC (Shizuoka, Japan). Mice were housed in the Experimental Animal Facility of Mie University. Mice were allowed to acclimatize for at least one week before being used for experiments. Mice were kept under specific-pathogen free conditions with 12-h light-dark cycles and were given access to bacteria-free food and water *ad libitum*. Animal

handling and experimental procedures were conducted in accordance with protocols approved by the Ethics Review Committee for Animal Experimentation of Mie University (#27-6-2).

4.2. Induction of Polymicrobial Sepsis

A mouse sepsis model was induced by the cecal ligation and puncture (CLP) procedure as previously described [69,70]. In brief, mice were anesthetized with isoflurane and underwent midline laparotomy. The position at 50% of the entire cecal length was ligated with 6-0 sterile nylon sutures (Natsume Seisakusho, Tokyo, Japan) and an 18-gauge needle (Terumo, Tokyo, Japan) was then inserted into the edge to make a single puncture. Mice in the control group were subjected only to laparotomy, but not to CLP procedures. In both the CLP and control groups, the incision was closed by suturing and the mice were then subcutaneously infused with 1 mL of sterile saline (0.9% sodium chloride). Administration of analgesics or antibiotics was avoided due to potential influences on altering mortality or immune responses in the CLP models [71,72].

4.3. Isolation of Peripheral Blood Mononuclear Cells (PBMCs)

PBMCs were isolated from the blood of septic mice 24 h after CLP as previously described with some modification [73]. Briefly, heparinized blood was incubated with ammonium-chloride-potassium (ACK) lysing buffer for 5 min. The cells were pelleted by centrifugation at $300\times g$ for 5 min, subjected to a resuspension in ACK buffer again, and processed as above. The cells pelleted were then washed twice with PBS by centrifugation at $300\times g$.

4.4. DSS-Induced Colitis

Mice were given 2.5% dextran sulfate sodium (DSS) (*w/v*, MW = 36,000–50,000; MP Biomedicals, Solon, OH, USA) in drinking water for seven days. Control mice were given DSS-free water. Inflammatory symptoms including body weight, bloody stool, rectal bleeding, and diarrhea were monitored daily.

4.5. EV Isolation via Differential Ultracentrifugation (UC)

EVs can be classified into three major subtypes—exosomes (30–150 nm), microvesicles (MVs) (50–1000 nm), and apoptotic bodies (ABs) (1–5 μm)—based on their size and biogenesis [74]. In this study, we isolated sEVs (exosomes) by eliminating MVs and ABs as described previously [75]. To avoid any confusion in nomenclature [76], we use the term “EVs” instead of exosomes or small EVs (sEVs); hereafter, the word “EVs” is used throughout this manuscript. EVs were isolated from gut-lavage fluids of control and CLP mice using differential UC as described previously with minor modifications [77]. In brief, mice were deprived of food 24 h prior to euthanasia and organ harvest. The luminal contents of the large and small intestines were obtained separately by gently flushing the lumen with phosphate-buffered saline (PBS). The lavage fluids were collected, pooled and subjected to sequential low- and high-speed centrifugation as follows. Three rounds of centrifugation at $1000\times g$ at 4 °C for 10 min were done to remove insoluble materials and debris. The supernatant was centrifuged three times at $5000\times g$ at 4 °C for 20 min to remove apoptotic bodies. To remove microvesicles, supernatant was transferred to ultracentrifuge tubes (Beckman Coulter, Brea, CA, USA) and centrifuged at $10,000\times g$ at 4 °C for 40 min using an L-60 ultracentrifuge (Beckman Coulter). Subsequently, the supernatant was transferred to new ultracentrifuge tubes and ultracentrifuged at $100,000\times g$ at 4 °C for 120 min. To purify the EV fraction, the pellet was resuspended in sterile PBS, filtered through a 0.22- μm Millex-GP syringe filter unit (Merck, Darmstadt, Germany) and ultracentrifuged again as described above. The EV pellet was resuspended in PBS and protein concentration was measured using the bicinchoninic acid (BCA) assay kit (Thermo Fisher Scientific, Waltham, MA, USA) with an iMarkTM Microplate Reader (Bio-Rad, Hercules, CA, USA) at 570 nm wavelength. EV samples were aliquoted and stored at $-80\text{ }^{\circ}\text{C}$ until use.

4.6. EV Isolation via Cushioned-Density Gradient Ultracentrifugation (C-DGUC)

In some experiments, C-DGUC was performed as described previously with some modifications [34,55]. In brief, gut-lavage fluids were pooled from sham or CLP mice (10 mice in each group) and concentrated into a final volume of 30 mL using the Amicon ultra-15 centrifugal filter unit (Merck) per the manufacturer's instructions. The concentrated samples were placed on 0.8 M and 2 M sucrose cushions and centrifuged at $100,000\times g$ for 120 min at 4 °C in an SW32Ti rotor using the L-80 ultracentrifuge (Beckman Coulter). The interface layer was harvested, diluted five-fold with HEPES buffered saline (HBS), filtered through the 0.22- μm filter unit (Merck) and then repeated for sucrose ultracentrifugation in a SW41Ti rotor as described above. The interface layer was harvested and diluted in 2.3 mL of HBS and mixed with an equal volume of 60% iodixanol to achieve a 30% iodixanol concentration containing EVs. This solution was overlaid with 20% and 5% iodixanol solutions and centrifuged at $200,000\times g$ for 120 min at 4 °C in an SW32Ti rotor. Ten consecutive 1-mL fractions were diluted in PBS and centrifuged at $100,000\times g$ for 120 min to pellet the EVs. Each pellet was resuspended in 100 μL of PBS and the protein concentration was measured as described above.

4.7. EV Measurements for Particle Size and Number

The particle size and concentration of isolated EVs were assessed using a NanoSight LM10 microscope and nanoparticle tracking analysis (NTA) software (Malvern panalytical, Malvern, UK) or by a dynamic light scattering (DLS) device (Horiba, Kyoto, Japan).

4.8. Flow Cytometry Analysis of EVs Conjugated to Microbeads

EVs were immobilized onto poly-L-lysine latex beads (4 μm) (Thermo Fisher Scientific) and stained with fluorophore-conjugated monoclonal antibodies as previously described [78]. Antibodies to CD63 (NVG-2), CD41 (MWRReg30), CD45 (30-F11), rat IgG2b isotype (RTK4530), and mouse IgG1 isotype (MOPC-21) were purchased from BioLegend (San Diego, CA, USA). Antibodies to CD9 (KMC8) and rat IgG2a isotype (R35-95) were obtained from BD Biosciences (San Jose, CA, USA). Antibody to EpCAM (G8.8) was purchased from eBioscience (San Diego, CA, USA). The stained EVs were analyzed using a BD AccuriTM C6 Flow Cytometer and BD Accuri C6 software (BD Biosciences).

4.9. Endotoxin Assay

EVs were tested for lipopolysaccharide (LPS) contamination using an ELISA kit (CUSABIO, Wuhan, China) according to the manufacturer's instructions. The LPS level of EVs at an equal protein concentration (0.5 mg/mL) was measured as previously described [55]. The optical densities and LPS concentrations were analyzed at dual wavelength absorbance (detection at 450 nm and correction at 570 nm) using an iMarkTM Microplate Reader (Bio-Rad).

4.10. Mouse Ileal-Loop Assay

The biological activity of CLP and control EVs on intestinal cells was assessed in vivo using a slightly modified protocol of the ileal loop assay in accordance with a previous report with slight modifications [79]. Briefly, a midline incision (laparotomy) was performed on 2.5% DSS-treated (for seven days) mice. An approximately 4 cm-long intestinal loop was made by double ligation of the ileum using 6-0 sterile nylon sutures (Natsume Seisakusho). The 50 μg of EVs were injected at a volume of 200 μL per loop using a 29-gauge needle (Terumo) [80]. In our preliminary study, mortality was recorded 20 h following ligation of ileal tissue in mice (data not shown). Therefore, for subsequent EV treatment into ligated ileal loops, mice were euthanized 18 h post-EV treatment as described previously [81] and ileal-loop tissues were harvested for further analysis.

4.11. Isolation, Culture, and EV Treatment of Mouse Primary Intestinal Epithelial Cells

Primary epithelial cells were isolated as described previously [82] with slight modifications. Briefly, small intestines were harvested from 4 mice, opened longitudinally, and washed extensively with RPMI1640 medium (Nacalai, Kyoto, Japan) after mesentery, fats, Peyer's patches, and luminal content were removed. The intestines were cut into pieces and shaken gently in RPMI-1640 containing EDTA (2 mM) and 10% fetal bovine serum (FBS) (Equitech-Bio, Kerrville, TX, USA). The tissue preparations were filtered with 70- μ m mesh filters. Using 25%, 40%, and 75% Percoll (GE Healthcare Life Sciences, Chicago, IL, USA), the whole cells were spun in a centrifuge (AX-511) (Tomy, Tokyo, Japan) at 780 \times g for 20 min and IECs were obtained from the interface between the 25% and 40% layers. After verification of their expression of epithelial marker, the IECs were seeded in 12-well culture plates (Corning, Glendale, AZ, USA) at 4×10^5 cells/mL in RPMI1640 containing penicillin/streptomycin and EV-depleted FBS and incubated at 37 °C with 5% CO₂ for 12 h. Then, the cells were treated with the indicated concentrations of EVs for 24 h after which RNA was extracted for further analysis.

4.12. EV miRNA Analysis via Deep Sequencing

Total RNA was extracted from EVs with TRIzol reagent (Thermo Fisher Scientific). Library construction of small RNAs (including miRNAs) was carried out using an Ion Total RNA-Seq Kit v2 (Thermo Fisher Scientific) according to the manufacturer's instructions at the Mie University Center for Molecular Biology and Genetics (Tsu, Japan). Sequencing of small RNA libraries was done using the Ion PGM system (Thermo Fisher Scientific) and data were collected using Torrent Suite v4.0.1 software. miRNA expression was shown as RPKM and miRNAs with a value of ≥ 1 RPKM were chosen to further assess their expressions [83]. Fold changes were calculated by taking the ratio of the individual miRNA expression values. Those miRNAs with value > 1 of \log_2 were classified as upregulated and those with < -1 as downregulated. In this measurements, the fold changes were shown with respect to the CLP group; thus, the miRNAs were upregulated or downregulated compared to the control group.

4.13. Gene Ontology (GO) Analysis

Target genes for upregulated miRNAs were selected based on annotations provided in the miRTarBase database (<http://mirtarbase.mbc.nctu.edu.tw/php/index.php>). Due to the large number of predicted targets, only those already validated by a wet lab experiment (with support type being functional) were retained and used for further study. Targets predicted from miRTarBase for the upregulated miRNAs and their targets were used to perform GO enrichment analysis using the online tool DAVID (<https://david.ncifcrf.gov/>). For each enrichment analysis, a set of all the known miRNA targets (as compiled in miRTarBase) was used as background in order to eliminate biases caused by non-specific enrichment of pathways resulting from miRNAs in general. The GO terms with a *p*-value of less than 0.05 were considered significant.

4.14. RT-qPCR

RNA (approximately 1 μ g per reaction) extracted from PBMCs, mouse ileal tissues, cultured primary IECs, or EVs using TRIzol reagent was subjected to a Prime Script RT reagent Kit (Takara Bio, Shiga, Japan) or a Mir-X miRNA First-Strand Synthesis Kit (Takara Bio) in order to detect the expressions of target genes and miRNAs, respectively, according to the manufacturers' instructions. To examine relative gene expression, qPCR was conducted using a PowerUp SYBR Green Master Mix PCR kit (Applied Biosystems, Foster City, CA, USA) and the StepOne Real-Time PCR System (Applied Biosystems) according to manufacturers' instructions. For endogenous controls, β -actin and U6 were used to normalize mRNA and miRNA expressions, respectively [78]. For miRNAs, universal primer for the reaction was utilized as the reverse primer (Thermo Fisher Scientific). The PCR primers used in this study are listed in Table S1. Relative expression was calculated using the comparative

threshold (CT) method ($2^{-\Delta\text{CT}}$ for mRNA and $2^{-\Delta\Delta\text{CT}}$ for miRNA) normalized to endogenous controls and expressed as the fold change between groups.

4.15. Statistical Analysis

Data are presented as the mean \pm standard error of the mean (SEM). Results were analyzed using two-tailed Student's *t*-test for comparison of two groups and one-way ANOVA when three or more groups were compared. *p*-values < 0.05 were considered significant. Statistical analysis was performed with Prism 8 software (GraphPad, San Diego, CA, USA).

Supplementary Materials: Supplementary materials can be found at <http://www.mdpi.com/1422-0067/21/22/8445/s1>. Figure S1. Monitoring of survival rates in mice following CLP or sham operation (laparotomy). Figure S2. RT-qPCR analysis for gene expression of proinflammatory mediators (PBMCs). Figure S3. Flow cytometry analysis of luminal EVs isolated from lavage fluids of small intestines. Figure S4. Flow cytometry analysis of luminal EVs isolated from lavage fluids of large intestines (C-DGUC method). Figure S5. Determination of bacterial endotoxin levels in EV samples. Figure S6. RT-qPCR analysis for relative gene expressions of TNF- α , IL-17A, IL-1 β , IL-6, and IL-22 in ileal-loop tissues of the healthy mice treated with EVs. Figure S7. RT-qPCR analysis for relative gene expressions of IL-1 β , IL-6, and IL-22 in ileal-loop tissues of the gut-inflamed mice treated with EVs. Figure S8. RT-qPCR analysis for relative gene expressions of TNF- α and IL-17A in ileal-loop tissues of the healthy mice treated with EVs isolated via C-DGUC method. Figure S9. Confirmation of EpCAM expression and analysis of EV effects on altering TNF- α and IL-17A expressions in mouse IECs. Figure S10. Gene Ontology enrichment analysis. Table S1. Primer sequences used in RT-qPCR. Table S2. All miRNAs detected, RPKM values, and fold changes. Table S3. RPKM values and fold change of miRNAs targeting TNF- α and IL-17A.

Author Contributions: M.G.A. mainly carried out experiments; E.J.P. and S.D. contributed to experiments; E.K., Y.A., and A.G. helped establish some assays; M.K. and S.A. helped analyze miRNAs; E.J.P. and M.S. designed the study and performed data interpretation; M.G.A., E.J.P., and M.S. wrote the manuscript. All authors read and approved the final manuscript.

Funding: This work was supported by Grants-in-Aid for Scientific Research from the Japan Society for the Promotion of Science (JSPS) (#18H02622 and #19K09392).

Acknowledgments: We are grateful to Jaewook Lee and Yong Song Gho for their technical advice on EV isolation. We also acknowledge Naohiro Seo, Fumiyasu Momose, and Hiroshi Shiku for technical support of EV measurement with NTA and DLS.

Conflicts of Interest: The authors declare no conflict of interest.

References

1. Singer, M.; Deutschman, C.S.; Seymour, C.C.; Shankar-Hari, M.M.; Annane, D.; Bauer, M.M.; Bellomo, R.; Bernard, G.R.; Chiche, J.D.J.; Coopersmith, C.C.; et al. The Third International Consensus Definitions for Sepsis and Septic Shock (Sepsis-3). *JAMA* **2016**, *315*, 801–810. [[CrossRef](#)] [[PubMed](#)]
2. Rudd, K.E.; Johnson, S.C.; Agesa, K.M.; Shackelford, K.A.; Tsoi, D.; Kievlan, D.R.; Colombara, D.V.; Ikuta, K.S.; Kisson, N.; Finfer, S.; et al. Global, regional, and national sepsis incidence and mortality, 1990–2017: Analysis for the Global Burden of Disease Study. *Lancet* **2020**, *395*, 200–211. [[CrossRef](#)]
3. Husain, K.D.; Coopersmith, C.M. Role of intestinal epithelial apoptosis in survival. *Curr. Opin. Crit. Care* **2003**, *9*, 159–163. [[CrossRef](#)] [[PubMed](#)]
4. Tamion, F.; Richard, V.; Lyoumi, S.; Daveau, M.; Bonmarchand, G.; Leroy, J.; Thuillez, C.; Lebreton, J.P. Gut ischemia and mesenteric synthesis of inflammatory cytokines after hemorrhagic or endotoxic shock. *Am. J. Physiol. Content* **1997**, *273*, G314–G321. [[CrossRef](#)] [[PubMed](#)]
5. Tamion, F.; Richard, V.; Sauger, F.; Menard, J.-F.; Girault, C.; Richard, J.; Thuillez, C.; Leroy, J.; Bonmarchand, G. Gastric mucosal acidosis and cytokine release in patients with septic shock. *Crit. Care Med.* **2003**, *31*, 2137–2143. [[CrossRef](#)]
6. Glatzle, J.; Kasparek, M.S.; Mueller, M.H.; Binder, F.; Meile, T.; Kreis, M.E.; Königsrainer, A.; Steurer, W. Enteral Immunonutrition During Sepsis Prevents Pulmonary Dysfunction in a Rat Model. *J. Gastrointest. Surg.* **2007**, *11*, 719–724. [[CrossRef](#)]
7. Glatzle, J.; Leutenegger, C.M.; Mueller, M.H.; Kreis, M.E.; Raybould, H.E.; Zittel, T.T. Mesenteric lymph collected during peritonitis or sepsis potentially inhibits gastric motility in rats. *J. Gastrointest. Surg.* **2004**, *8*, 645–652. [[CrossRef](#)]

8. Königsrainer, I.; Türck, M.H.; Eisner, F.; Meile, T.; Hoffmann, J.; Küper, M.; Zieker, D.; Glatzle, J. The Gut is not only the Target but a Source of Inflammatory Mediators Inhibiting Gastrointestinal Motility during Sepsis. *Cell. Physiol. Biochem.* **2011**, *28*, 753–760. [[CrossRef](#)]
9. Zhang, Y.-M. Intravenous infusion of mesenteric lymph from severe intraperitoneal infection rats causes lung injury in healthy rats. *World J. Gastroenterol.* **2014**, *20*, 4771–4777. [[CrossRef](#)]
10. Deitch, E.A. Gut-origin sepsis: Evolution of a concept. *Surge* **2012**, *10*, 350–356. [[CrossRef](#)]
11. Klingensmith, N.J.; Coopersmith, C.M. The Gut as the Motor of Multiple Organ Dysfunction in Critical Illness. *Crit. Care Clin.* **2016**, *32*, 203–212. [[CrossRef](#)] [[PubMed](#)]
12. Yang, C.C.; Ogawa, H.; Dwinell, M.B.; McCole, D.F.; Eckmann, L.; Kagnoff, M.F. Chemokine receptor CCR6 transduces signals that activate p130Cas and alter cAMP-stimulated ion transport in human intestinal epithelial cells. *Am. J. Physiol. Physiol.* **2005**, *288*, C321–C328. [[CrossRef](#)] [[PubMed](#)]
13. Parikh, A.A.; Salzman, A.L.; Fischer, J.E.; Szabo, C.; Hasselgren, P.O. Interleukin-1 beta and interferon-gamma regulate interleukin-6 production in cultured human intestinal epithelial cells. *Shock* **1997**, *8*, 249–255. [[CrossRef](#)]
14. Sonnier, D.I.; Bailey, S.R.; Schuster, R.M.; Gangidine, M.M.; Lentsch, A.B.; Pritts, T.A. Proinflammatory Chemokines in the Intestinal Lumen Contribute to Intestinal Dysfunction during Endotoxemia. *Shock* **2012**, *37*, 63–69. [[CrossRef](#)] [[PubMed](#)]
15. Simons, M.; Raposo, G. Exosomes—Vesicular carriers for intercellular communication. *Curr. Opin. Cell Biol.* **2009**, *21*, 575–581. [[CrossRef](#)] [[PubMed](#)]
16. Valadi, H.; Ekström, K.; Bossios, A.; Sjöstrand, M.; Lee, J.J.; Tvall, J.O.L.O. Exosome-mediated transfer of mRNAs and microRNAs is a novel mechanism of genetic exchange between cells. *Nat. Cell Biol.* **2007**, *9*, 654–659. [[CrossRef](#)]
17. Miksa, M.; Wu, R.; Dong, W.; Komura, H.; Amin, D.; Ji, Y.; Wang, Z.; Wang, H.; Ravikumar, T.S.; Tracey, K.J.; et al. Immature dendritic cell-derived exosomes rescue septic animals via milk fat globule epidermal growth factor-factor VIII. *J. Immunol.* **2009**, *183*, 5983–5990. [[CrossRef](#)]
18. Xu, J.; Feng, Y.; Jeyaram, A.; Jay, S.M.; Zou, L.; Chao, W. Circulating Plasma Extracellular Vesicles from Septic Mice Induce Inflammation via MicroRNA- and TLR7-Dependent Mechanisms. *J. Immunol.* **2018**, *201*, 3392–3400. [[CrossRef](#)]
19. Zhang, X.; Wang, X.; Fan, M.; Tu, F.; Yang, K.; Ha, T.; Liu, L.; Kalbfleisch, J.; Williams, D.; Li, C. Endothelial HSPA12B Exerts Protection Against Sepsis-Induced Severe Cardiomyopathy via Suppression of Adhesion Molecule Expression by miR-126. *Front. Immunol.* **2020**, *11*, 566. [[CrossRef](#)]
20. Real, J.M.; Ferreira, L.R.P.; Esteves, G.H.; Koyama, F.C.; Dias, M.V.S.; Bezerra-Neto, J.E.; Cunha-Neto, E.; Machado, F.R.; Salomao, R.; Azevedo, L.C.P. Exosomes from patients with septic shock convey miRNAs related to inflammation and cell cycle regulation: New signaling pathways in sepsis? *Crit. Care* **2018**, *22*, 1–11. [[CrossRef](#)]
21. Kawamoto, E.; Masui-Ito, A.; Eguchi, A.; Soe, Z.Y.; Prajuabjinda, O.; Darkwah, S.; Park, E.J.; Imai, H.; Shimaoka, M. Integrin and PD-1 Ligand Expression on Circulating Extracellular Vesicles in Systemic Inflammatory Response Syndrome and Sepsis. *Shock* **2019**, *52*, 13–22. [[CrossRef](#)] [[PubMed](#)]
22. Chen, X.; Song, C.H.; Feng, B.S.; Li, T.L.; Li, P.; Zheng, P.Y.; Chen, X.M.; Xing, Z.; Yang, P.C. Intestinal epithelial cell-derived integrin alpha6 plays an important role in the induction of regulatory T cells and inhibits an antigen-specific Th2 response. *J. Leukoc. Biol.* **2011**, *90*, 751–759. [[CrossRef](#)] [[PubMed](#)]
23. Kojima, M.; Costantini, T.W.; Eliceiri, B.; Chan, T.W.; Baird, A.; Coimbra, R. Gut epithelial cell-derived exosomes trigger posttrauma immune dysfunction. *J. Trauma Acute Care Surg.* **2018**, *84*, 257–264. [[CrossRef](#)] [[PubMed](#)]
24. Hu, G.; Gong, A.-Y.; Roth, A.L.; Huang, B.Q.; Ward, H.D.; Zhu, G.; LaRusso, N.F.; Hanson, N.D.; Chen, X.-M. Release of Luminal Exosomes Contributes to TLR4-Mediated Epithelial Antimicrobial Defense. *PLoS Pathog.* **2013**, *9*, e1003261. [[CrossRef](#)] [[PubMed](#)]
25. Deng, Z.-B.; Zhuang, X.; Ju, S.; Xiang, X.; Mu, J.; Liu, Y.; Jiang, H.; Zhang, L.; Mobley, J.; McClain, C.; et al. Exosome-like nanoparticles from intestinal mucosal cells carry prostaglandin E2 and suppress activation of liver NKT cells. *J. Immunol.* **2013**, *190*, 3579–3589. [[CrossRef](#)] [[PubMed](#)]
26. Mitsuhashi, S.; Feldbrügge, L.; Csizmadia, E.; Mitsuhashi, M.; Robson, S.C.; Moss, A.C. Luminal Extracellular Vesicles (EVs) in Inflammatory Bowel Disease (IBD) Exhibit Proinflammatory Effects on Epithelial Cells and Macrophages. *Inflamm. Bowel Dis.* **2016**, *22*, 1587–1595. [[CrossRef](#)] [[PubMed](#)]

27. Teixeira-Da-Cunha, M.G.A.; Gomes, R.N.; Roehrs, N.; Bozza, F.A.; Prescott, S.M.; Stafforini, D.; Zimmerman, G.A.; Bozza, P.T.; Castro-Faria-Neto, H.C. Bacterial Clearance Is Improved in Septic Mice by Platelet-Activating Factor-Acetylhydrolase (PAF-AH) Administration. *PLoS ONE* **2013**, *8*, e74567. [[CrossRef](#)]
28. Chaudhry, H.; Zhou, J.; Zhong, Y.; Ali, M.M.; McGuire, F.; Nagarkatti, P.S.; Nagarkatti, M. Role of cytokines as a double-edged sword in sepsis. *Vivo* **2013**, *27*, 669–684.
29. Shalova, I.N.; Lim, J.Y.; Chittechath, M.; Zinkernagel, A.S.; Beasley, F.; Hernández-Jiménez, E.; Toledano, V.; Cubillos-Zapata, C.; Rapisarda, A.; Chen, J.; et al. Human Monocytes Undergo Functional Re-programming during Sepsis Mediated by Hypoxia-Inducible Factor-1 α . *Immunity* **2015**, *42*, 484–498. [[CrossRef](#)]
30. Schuijt, T.J.; Van Der Poll, T.; De Vos, W.M.; Wiersinga, W.J. The intestinal microbiota and host immune interactions in the critically ill. *Trends Microbiol.* **2013**, *21*, 221–229. [[CrossRef](#)]
31. Wu, Y.; Chung, C.-S.; Chen, Y.; Monaghan, S.F.; Patel, S.; Huang, X.; Heffernan, D.S.; Ayala, A. A Novel Role for Programmed Cell Death Receptor Ligand-1 in Sepsis-Induced Intestinal Dysfunction. *Mol. Med.* **2016**, *22*, 830–840. [[CrossRef](#)] [[PubMed](#)]
32. Alex, P.; Zachos, N.C.; Nguyen, T.; Gonzales, L.; Chen, T.E.; Conklin, L.S.; Centola, M.; Li, X. Distinct Cytokine Patterns Identified from Multiplex Profiles of Murine DSS and TNBS-Induced Colitis. *Inflamm. Bowel Dis.* **2009**, *15*, 341–352. [[CrossRef](#)] [[PubMed](#)]
33. Strober, W.; Fuss, I.J. Proinflammatory Cytokines in the Pathogenesis of Inflammatory Bowel Diseases. *Gastroenterology* **2011**, *140*, 1756–1767.e1. [[CrossRef](#)] [[PubMed](#)]
34. Li, K.; Wong, D.K.; Hong, K.Y.; Raffai, R.L. Cushioned-Density Gradient Ultracentrifugation (C-DGUC): A Refined and High Performance Method for the Isolation, Characterization, and Use of Exosomes. *Cytokine Bioassays* **2018**, *1740*, 69–83. [[CrossRef](#)]
35. Duong, P.; Chung, A.; Bouchareychas, L.; Raffai, R.L. Cushioned-Density Gradient Ultracentrifugation (C-DGUC) improves the isolation efficiency of extracellular vesicles. *PLoS ONE* **2019**, *14*, e0215324. [[CrossRef](#)]
36. Raeven, P.; Zipperle, J.; Drechsler, S. Extracellular Vesicles as Markers and Mediators in Sepsis. *Theranostics* **2018**, *8*, 3348–3365. [[CrossRef](#)]
37. Park, E.J.; Appiah, M.G.; Myint, P.K.; Gaowa, A.; Kawamoto, E.; Shimaoka, M. Exosomes in Sepsis and Inflammatory Tissue Injury. *Curr. Pharm. Des.* **2020**, *25*, 4486–4495. [[CrossRef](#)]
38. Kagnoff, M.F. The intestinal epithelium is an integral component of a communications network. *J. Clin. Investig.* **2014**, *124*, 2841–2843. [[CrossRef](#)]
39. Chen, G.-Y.; Chen, X.; King, S.; Cavassani, K.A.; Cheng, J.; Zheng, X.; Cao, H.; Yu, H.; Qu, J.; Fang, D.; et al. Amelioration of sepsis by inhibiting sialidase-mediated disruption of the CD24-SiglecG interaction. *Nat. Biotechnol.* **2011**, *29*, 428–435. [[CrossRef](#)]
40. Haussner, F.; Chakraborty, S.; Halbgebauer, R.; Huber-Lang, M.S. Challenge to the Intestinal Mucosa during Sepsis. *Front. Immunol.* **2019**, *10*, 891. [[CrossRef](#)]
41. Azevedo, L.C.P.; Janiszewski, M.; Pontieri, V.; Pedro, M.D.A.; Bassi, E.; Tucci, P.J.F.; Laurindo, F.R. Platelet-derived exosomes from septic shock patients induce myocardial dysfunction. *Crit. Care* **2007**, *11*, R120. [[CrossRef](#)] [[PubMed](#)]
42. Essandoh, K.; Yang, L.; Wang, X.; Huang, W.; Qin, D.; Hao, J.; Wang, Y.; Zingarelli, B.; Peng, T.; Fan, G.-C. Blockade of exosome generation with GW4869 dampens the sepsis-induced inflammation and cardiac dysfunction. *Biochim. Biophys. Acta (BBA) Mol. Basis Dis.* **2015**, *1852*, 2362–2371. [[CrossRef](#)] [[PubMed](#)]
43. Mu, X.; Wang, X.; Huang, W.; Wang, R.-T.; Essandoh, K.; Li, Y.; Pugh, A.M.; Peng, J.; Deng, S.; Wang, Y.; et al. Circulating Exosomes Isolated from Septic Mice Induce Cardiovascular Hyperpermeability Through Promoting Podosome Cluster Formation. *Shock* **2018**, *49*, 429–441. [[CrossRef](#)] [[PubMed](#)]
44. Jiang, K.; Yang, J.; Guo, S.; Zhao, G.; Wu, H.; Deng, G. Peripheral Circulating Exosome-Mediated Delivery of miR-155 as a Novel Mechanism for Acute Lung Inflammation. *Mol. Ther.* **2019**, *27*, 1758–1771. [[CrossRef](#)] [[PubMed](#)]
45. Gao, K.; Jin, J.; Huang, C.; Li, J.; Luo, H.; Li, L.; Huang, Y.; Jiang, Y. Exosomes Derived from Septic Mouse Serum Modulate Immune Responses via Exosome-Associated Cytokines. *Front. Immunol.* **2019**, *10*, 1560. [[CrossRef](#)] [[PubMed](#)]
46. Deng, J.-N.; Li, Y.-Q.; Liu, Y.; Li, Q.; Hu, Y.; Xu, J.-Q.; Sun, T.-Y.; Xie, L.X. Exosomes derived from plasma of septic patients inhibit apoptosis of T lymphocytes by down-regulating bad via hsa-miR-7-5p. *Biochem. Biophys. Res. Commun.* **2019**, *513*, 958–966. [[CrossRef](#)] [[PubMed](#)]

47. Roulis, M.; Armaka, M.; Manoloukos, M.; Apostolaki, M.; Kollias, G. Intestinal epithelial cells as producers but not targets of chronic TNF suffice to cause murine Crohn-like pathology. *Proc. Natl. Acad. Sci. USA* **2011**, *108*, 5396–5401. [[CrossRef](#)]
48. Takahashi, N.; Vanlaere, I.; De Rycke, R.; Cauwels, A.; Joosten, L.A.; Lubberts, E.; Berg, W.B.V.D.; Libert, C. IL-17 produced by Paneth cells drives TNF-induced shock. *J. Exp. Med.* **2008**, *205*, 1755–1761. [[CrossRef](#)]
49. Kojima, M.; Gimenes-Junior, J.A.; Chan, T.W.; Eliceiri, B.P.; Baird, A.; Costantini, T.W.; Coimbra, R. Exosomes in postshock mesenteric lymph are key mediators of acute lung injury triggering the macrophage activation via Toll-like receptor 4. *FASEB J.* **2017**, *32*, 97–110. [[CrossRef](#)]
50. Wang, Y.; Shen, Y.; Liu, H.; Yin, J.; Zhang, X.-T.; Gong, A.-Y.; Chen, X.; Chen, S.; Mathy, N.W.; Cao, J.; et al. Induction of Inflammatory Responses in Splenocytes by Exosomes Released from Intestinal Epithelial Cells following *Cryptosporidium parvum* Infection. *Infect. Immun.* **2019**, *87*, 4. [[CrossRef](#)]
51. Haak, B.W.; Wiersinga, W.J. The role of the gut microbiota in sepsis. *Lancet Gastroenterol. Hepatol.* **2017**, *2*, 135–143. [[CrossRef](#)]
52. Adelman, M.W.; Woodworth, M.H.; Langelier, C.; Busch, L.M.; Kempker, J.A.; Kraft, C.S.; Martin, G.S. The gut microbiome's role in the development, maintenance, and outcomes of sepsis. *Crit. Care* **2020**, *24*, 1–10. [[CrossRef](#)] [[PubMed](#)]
53. Murao, A.; Brenner, M.; Aziz, M.; Wang, P. Exosomes in Sepsis. *Front. Immunol.* **2020**, *11*, 2140. [[CrossRef](#)] [[PubMed](#)]
54. Bassetti, M.; Bandera, A.; Gori, A. Therapeutic Potential of the Gut Microbiota in the Management of Sepsis. *Crit. Care* **2020**, *24*, 1–7. [[CrossRef](#)]
55. Park, K.-S.; Lee, J.; Lee, C.; Park, H.T.; Kim, J.-W.; Kim, O.Y.; Kim, S.R.; Rådinger, M.; Jung, H.-Y.; Park, J.; et al. Sepsis-Like Systemic Inflammation Induced by Nano-Sized Extracellular Vesicles from Feces. *Front. Microbiol.* **2018**, *9*, 1735. [[CrossRef](#)]
56. Liu, S.; Da Cunha, A.P.; Rezende, R.M.; Cialic, R.; Wei, Z.; Bry, L.; Comstock, L.E.; Gandhi, R.; Weiner, H.L. The Host Shapes the Gut Microbiota via Fecal MicroRNA. *Cell Host Microbe* **2016**, *19*, 32–43. [[CrossRef](#)]
57. Yin, N.; Yang, Y.; Wang, X.; Yang, C.; Ma, X.; Shaikat, A.; Zhao, G.; Deng, G. MiR-19a mediates the negative regulation of the NF-kappaB pathway in lipopolysaccharide-induced endometritis by targeting TBK1. *Inflamm. Res.* **2019**, *68*, 231–240. [[CrossRef](#)]
58. Yang, Q.; Zhang, D.; Li, Y.; Li, Y.; Li, Y. Paclitaxel alleviated liver injury of septic mice by alleviating inflammatory response via microRNA-27a/TAB3/NF-kappaB signaling pathway. *Biomed. Pharmacother.* **2018**, *97*, 1424–1433. [[CrossRef](#)]
59. Wang, Z.; Ruan, Z.; Mao, Y.; Dong, W.; Zhang, Y.; Yin, N.; Jiang, L. miR-27a is up regulated and promotes inflammatory response in sepsis. *Cell. Immunol.* **2014**, *290*, 190–195. [[CrossRef](#)]
60. Jia, P.; Wu, X.; Dai, Y.; Teng, J.; Fang, Y.; Hu, J.; Zou, J.; Liang, M.; Ding, X. MicroRNA-21 Is Required for Local and Remote Ischemic Preconditioning in Multiple Organ Protection Against Sepsis*. *Crit. Care Med.* **2017**, *45*, e703–e710. [[CrossRef](#)]
61. Wu, X.; Liu, Z.; Hu, L.; Gu, W.; Zhu, L. Exosomes derived from endothelial progenitor cells ameliorate acute lung injury by transferring miR-126. *Exp. Cell Res.* **2018**, *370*, 13–23. [[CrossRef](#)] [[PubMed](#)]
62. Zhou, Y.; Li, P.; Goodwin, A.J.; Cook, J.A.; Halushka, P.V.; Chang, E.; Fan, H. Exosomes from Endothelial Progenitor Cells Improve the Outcome of a Murine Model of Sepsis. *Mol. Ther.* **2018**, *26*, 1375–1384. [[CrossRef](#)] [[PubMed](#)]
63. He, R.; Li, Y.; Zhou, L.; Su, X.; Li, Y.; Pan, P.; Hu, C. miR-146b overexpression ameliorates lipopolysaccharide-induced acute lung injury in vivo and in vitro. *J. Cell. Biochem.* **2018**, *120*, 2929–2939. [[CrossRef](#)] [[PubMed](#)]
64. Tu, Z.; Xiong, J.; Xiao, R.; Shao, L.; Yang, X.; Zhou, L.; Yuan, W.; Wang, M.; Yin, Q.; Wu, Y.; et al. Loss of miR-146b-5p promotes T cell acute lymphoblastic leukemia migration and invasion via the IL-17A pathway. *J. Cell. Biochem.* **2018**, *120*, 5936–5948. [[CrossRef](#)] [[PubMed](#)]
65. Wendlandt, E.B.; Graff, J.W.; Gioannini, T.L.; McCaffrey, A.P.; Wilson, M.E. The role of microRNAs miR-200b and miR-200c in TLR4 signaling and NF-kappaB activation. *Innate Immun.* **2012**, *18*, 846–855. [[CrossRef](#)] [[PubMed](#)]

66. Bollrath, J.; Phesse, T.J.; Von Burstin, V.A.; Putoczki, T.; Bennecke, M.; Bateman, T.; Nebelsiek, T.; Lundgren-May, T.; Canli, Ö.; Schwitalla, S.; et al. gp130-Mediated Stat3 Activation in Enterocytes Regulates Cell Survival and Cell-Cycle Progression during Colitis-Associated Tumorigenesis. *Cancer Cell* **2009**, *15*, 91–102. [[CrossRef](#)] [[PubMed](#)]
67. Brand, S.; Beigel, F.; Olszak, T.; Zitzmann, K.; Eichhorst, S.T.; Otte, J.-M.; Diepolder, H.; Marquardt, A.; Jagla, W.; Popp, A.; et al. IL-22 is increased in active Crohn's disease and promotes proinflammatory gene expression and intestinal epithelial cell migration. *Am. J. Physiol. Liver Physiol.* **2006**, *290*, G827–G838. [[CrossRef](#)] [[PubMed](#)]
68. Kuhn, K.A.; Manieri, N.A.; Liu, T.-C.; Stappenbeck, T.S. IL-6 Stimulates Intestinal Epithelial Proliferation and Repair after Injury. *PLoS ONE* **2014**, *9*, e114195. [[CrossRef](#)]
69. Cuenca, A.G.; Delano, M.J.; Kelly-Scumpia, K.M.; Moldawer, L.L.; Efron, P.A. Cecal Ligation and Puncture. *Curr. Protoc. Immunol.* **2010**, *91*, 19.13.1–19.13.11. [[CrossRef](#)]
70. Darkwah, S.; Nago, N.; Appiah, M.G.; Myint, P.K.; Kawamoto, E.; Shimaoka, M.; Park, E.J. Differential Roles of Dendritic Cells in Expanding CD4 T Cells in Sepsis. *Biomedicines* **2019**, *7*, 52. [[CrossRef](#)]
71. Hugunin, K.M.; Fry, C.; Shuster, K.; Nemzek, J.A. Effects of Tramadol and Buprenorphine on Select Immunologic Factors in a Cecal Ligation and Puncture Model. *Shock* **2010**, *34*, 250–260. [[CrossRef](#)] [[PubMed](#)]
72. Lewis, A.J.; Seymour, C.W.; Rosengart, M.R. Current Murine Models of Sepsis. *Surg. Infect.* **2016**, *17*, 385–393. [[CrossRef](#)] [[PubMed](#)]
73. Dagur, P.K.; McCoy, J.P., Jr. Collection, Storage, and Preparation of Human Blood Cells. *Curr. Protoc. Cytom.* **2015**, *73*, 5.1.1–5.1.16. [[CrossRef](#)] [[PubMed](#)]
74. Crescitelli, R.; Lässer, C.; Szabó, T.G.; Kittel, A.; Eldh, M.; Dianzani, I.; Buzás, E.I.; Lötvall, J. Distinct RNA profiles in subpopulations of extracellular vesicles: Apoptotic bodies, microvesicles and exosomes. *J. Extracell. Vesicles* **2013**, *2*, 2. [[CrossRef](#)]
75. Théry, C.; Ostrowski, M.; Segura, E. Membrane vesicles as conveyors of immune responses. *Nat. Rev. Immunol.* **2009**, *9*, 581–593. [[CrossRef](#)]
76. Witwer, K.W.; Théry, C. Extracellular vesicles or exosomes? On primacy, precision, and popularity influencing a choice of nomenclature. *J. Extracell. Vesicles* **2019**, *8*, 1648167. [[CrossRef](#)]
77. Théry, C.; Amigorena, S.; Raposo, G.; Clayton, A. Isolation and Characterization of Exosomes from Cell Culture Supernatants and Biological Fluids. *Curr. Protoc. Cell Biol.* **2006**, *30*, 3.22.1–3.22.29. [[CrossRef](#)]
78. Park, E.J.; Prajuabjinda, O.; Soe, Z.Y.; Darkwah, S.; Appiah, M.G.; Kawamoto, E.; Momose, F.; Shiku, H.; Shimaoka, M. Exosomal regulation of lymphocyte homing to the gut. *Blood Adv.* **2019**, *3*, 1–11. [[CrossRef](#)]
79. Caserta, J.A.; Robertson, S.L.; Saputo, J.; Shrestha, A.; McClane, B.A.; Uzal, F.A. Development and Application of a Mouse Intestinal Loop Model to Study the In Vivo Action of Clostridium perfringens Enterotoxin. *Infect. Immun.* **2011**, *79*, 3020–3027. [[CrossRef](#)]
80. Fukuda, S.; Hase, K.; Ohno, H. Application of a Mouse Ligated Peyer's Patch Intestinal Loop Assay to Evaluate Bacterial Uptake by M cells. *J. Vis. Exp.* **2011**, e3225. [[CrossRef](#)]
81. Sawasvirojwong, S.; Srimanote, P.; Chatsudthipong, V.; Muanprasat, C. An Adult Mouse Model of Vibrio cholerae-induced Diarrhea for Studying Pathogenesis and Potential Therapy of Cholera. *PLoS Negl. Trop. Dis.* **2013**, *7*, e2293. [[CrossRef](#)] [[PubMed](#)]
82. Lee, J.; Park, E.J.; Yuki, Y.; Ahmad, S.; Mizuguchi, K.; Ishii, K.J.; Shimaoka, M.; Kiyono, H. Profiles of microRNA networks in intestinal epithelial cells in a mouse model of colitis. *Sci. Rep.* **2015**, *5*, 18174. [[CrossRef](#)] [[PubMed](#)]
83. Mai, Z.; Xiao, C.; Jin, J.; Zhang, G. Low-cost, Low-bias and Low-input RNA-seq with High Experimental Verifiability based on Semiconductor Sequencing. *Sci. Rep.* **2017**, *7*, 1053. [[CrossRef](#)] [[PubMed](#)]

Publisher's Note: MDPI stays neutral with regard to jurisdictional claims in published maps and institutional affiliations.



© 2020 by the authors. Licensee MDPI, Basel, Switzerland. This article is an open access article distributed under the terms and conditions of the Creative Commons Attribution (CC BY) license (<http://creativecommons.org/licenses/by/4.0/>).

Figure S1

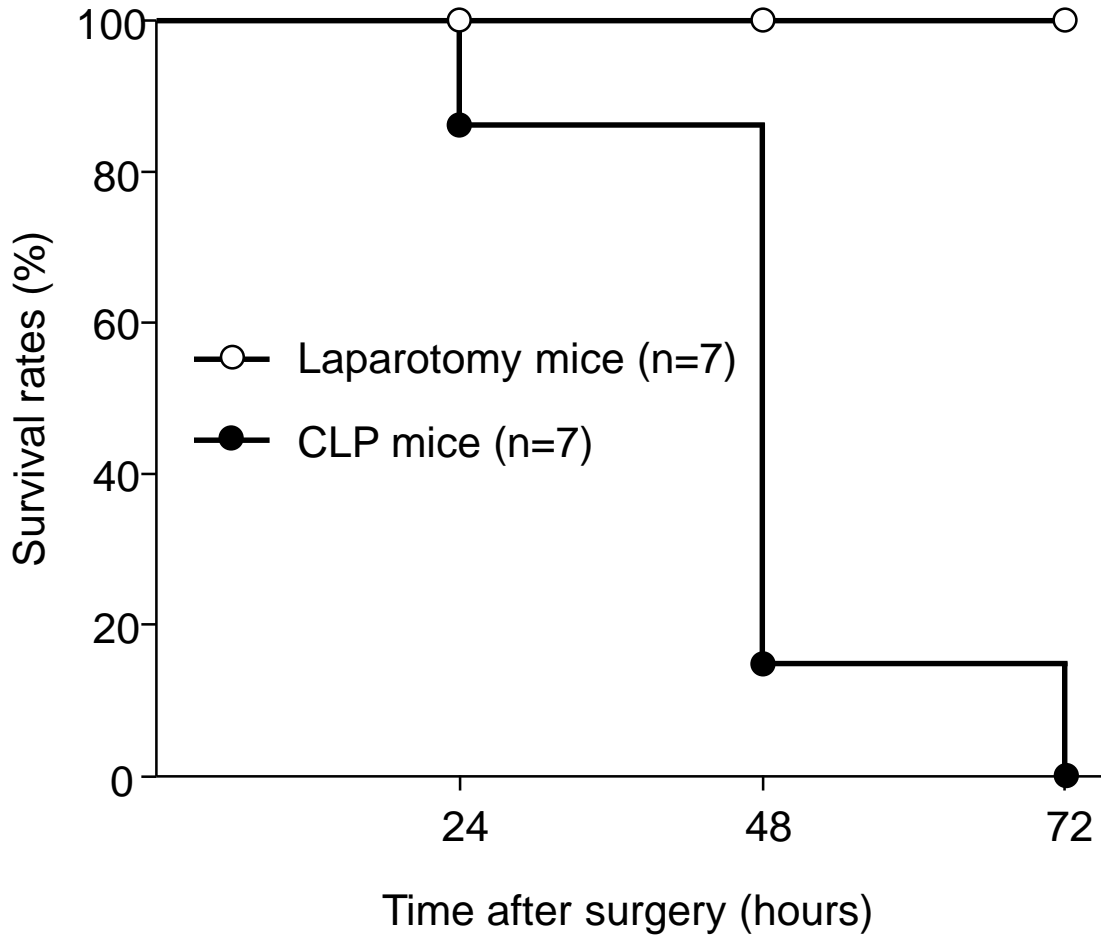


Figure S1. Monitoring of survival rates in mice following CLP or sham operation (laparotomy). Mortality of mice was observed for 72 hours. CLP (n=7) and laparotomy (n=7) mice were used in this assay.

Figure S2

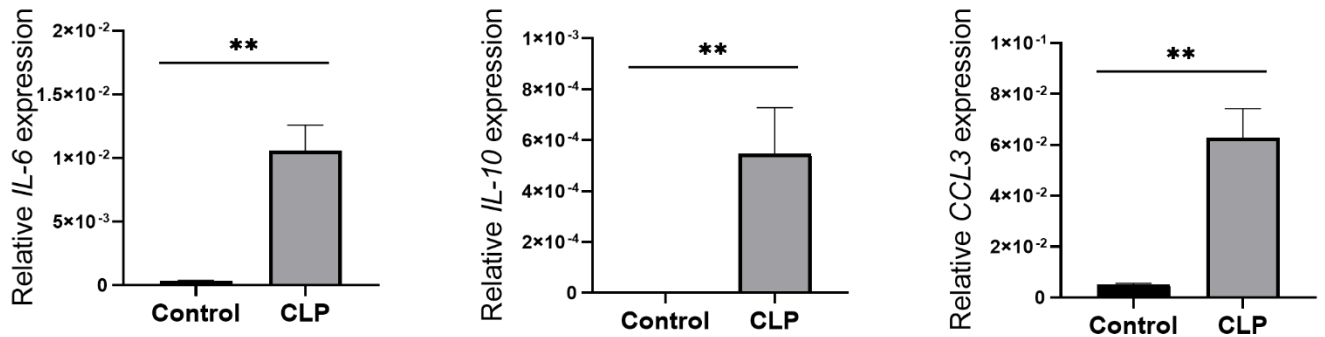


Figure S2. RT-qPCR analysis for gene expression. PBMCs were isolated from sham-operated control and CLP mice. RNA was extracted from the cells and analyzed for mRNA expression of the genes indicated. Relative expression of *IL-6*, *IL-10*, and *CCL3* to β -actin using $2^{-\Delta CT}$ method. Statistical significance was obtained by unpaired two-tailed t test. Whole blood from 3 mice was pooled, resulting in 4 blood samples per group (N=12). Extracted RNA was subjected to RT-qPCR assay. Results are shown as the mean \pm SEM. ** $p < 0.01$.

Figure S3

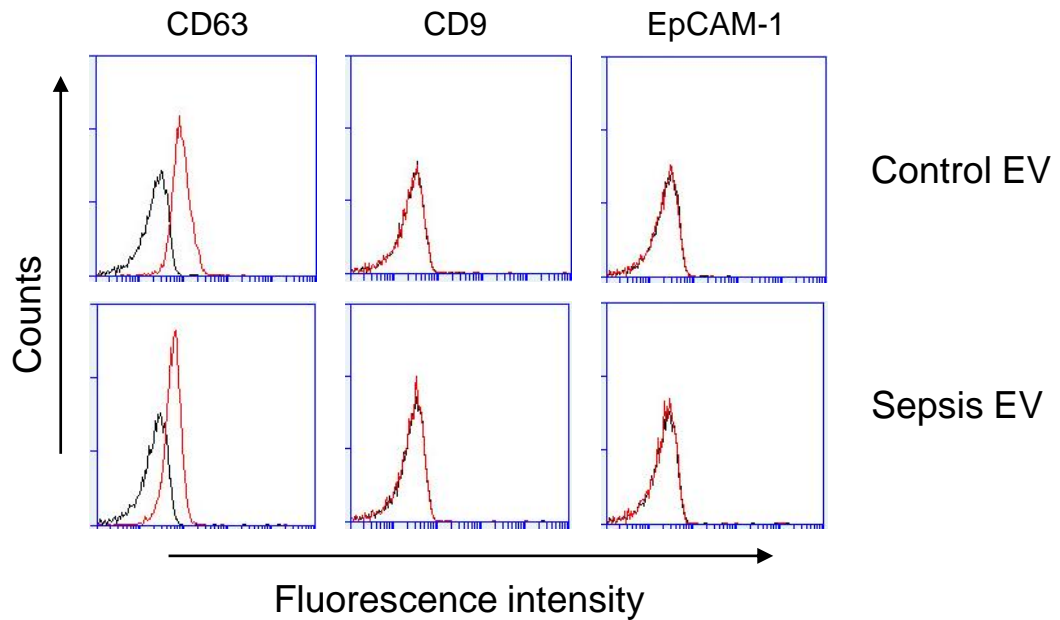


Figure S3. Flow cytometry analysis of luminal EVs isolated from control and septic mice. EVs were isolated from lavage fluids in small intestines of control and sepsis mice using differential UC. EVs were then adsorbed on 4 μm poly-L-lysine microbeads overnight. Immobilized EVs (20 μg) were stained with antibodies to mouse CD63, CD9, and EpCAM-1 and subjected to flow cytometry to evaluate their expression. Representative histograms show changes in expression of indicated markers. Black lines, isotype control; and red lines, monoclonal antibody (MAb).

Figure S4

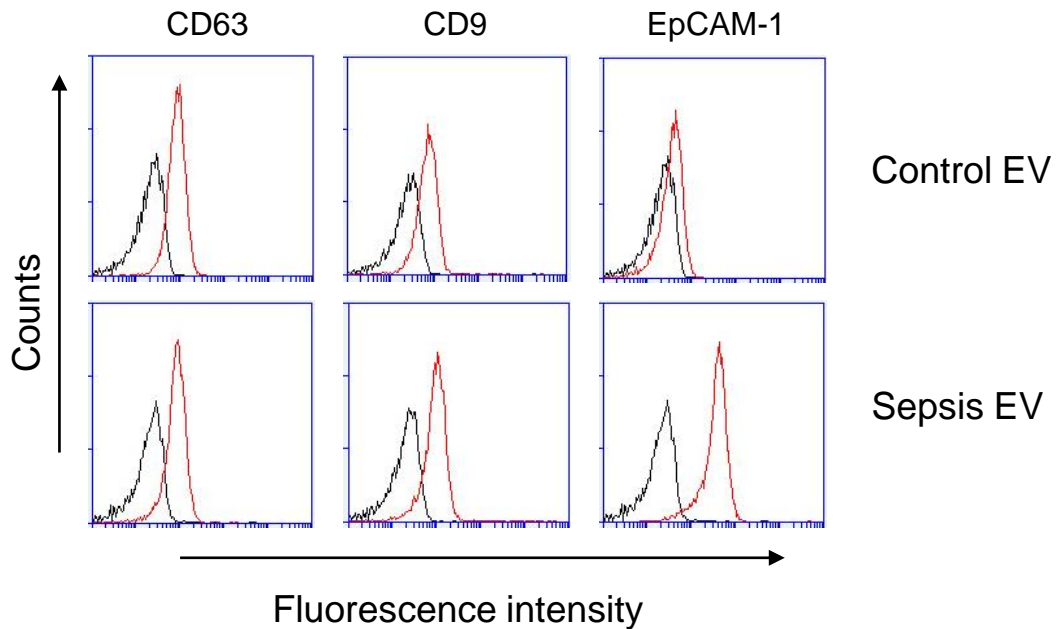


Figure S4. Flow cytometry analysis of luminal EVs isolated from large intestines of control and septic mice using C-DGUC. EVs were then adsorbed on 4 μm poly-L-lysine microbeads overnight. Immobilized EVs (20 μg) were stained with antibodies to mouse CD63, CD9, and EpCAM-1 and subjected to flow cytometry to evaluate their expression. Representative histograms show changes in the expression levels of the indicated markers. Black lines, isotype control; and red lines, monoclonal antibody (MAb).

Figure S5

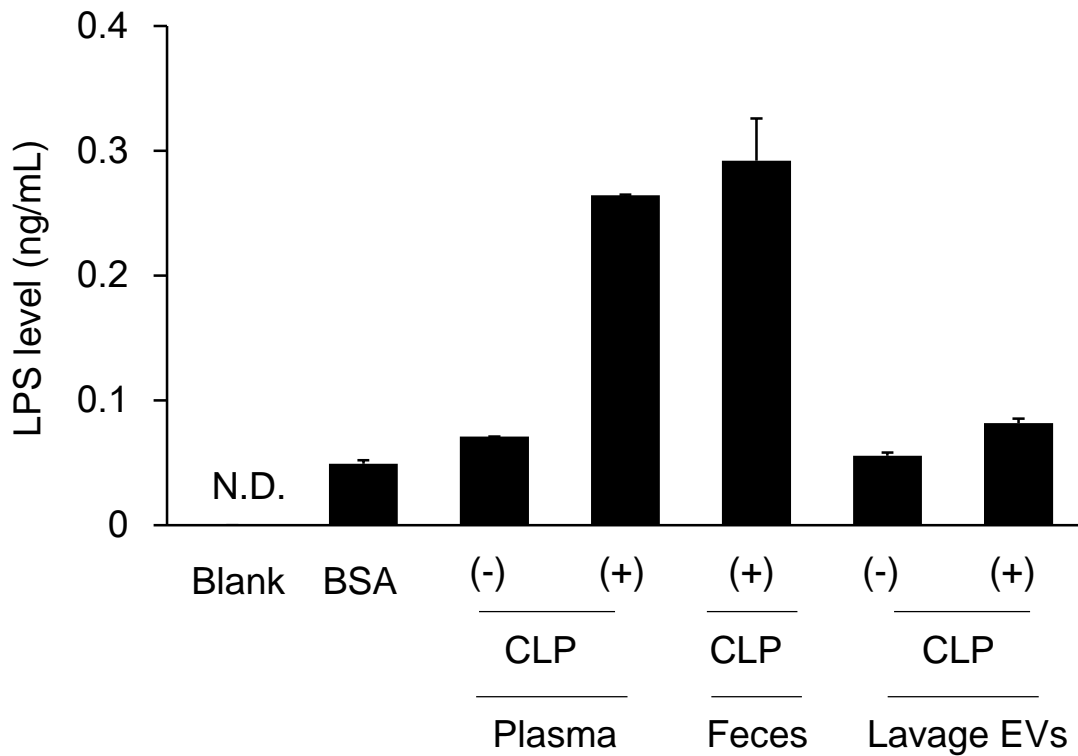


Figure S5. Determination of bacterial endotoxin (lipopolysaccharide; LPS) levels in EV samples. The EV samples were applied to an antibody-coated ELISA plate and analyzed for lipid A content. All samples had an equal concentration of 0.5 mg/ml. BSA was used as a negative control. Bar graphs represent the mean \pm SEM obtained from 2-5 mice per group. BSA, bovine serum albumin.

Figure S6

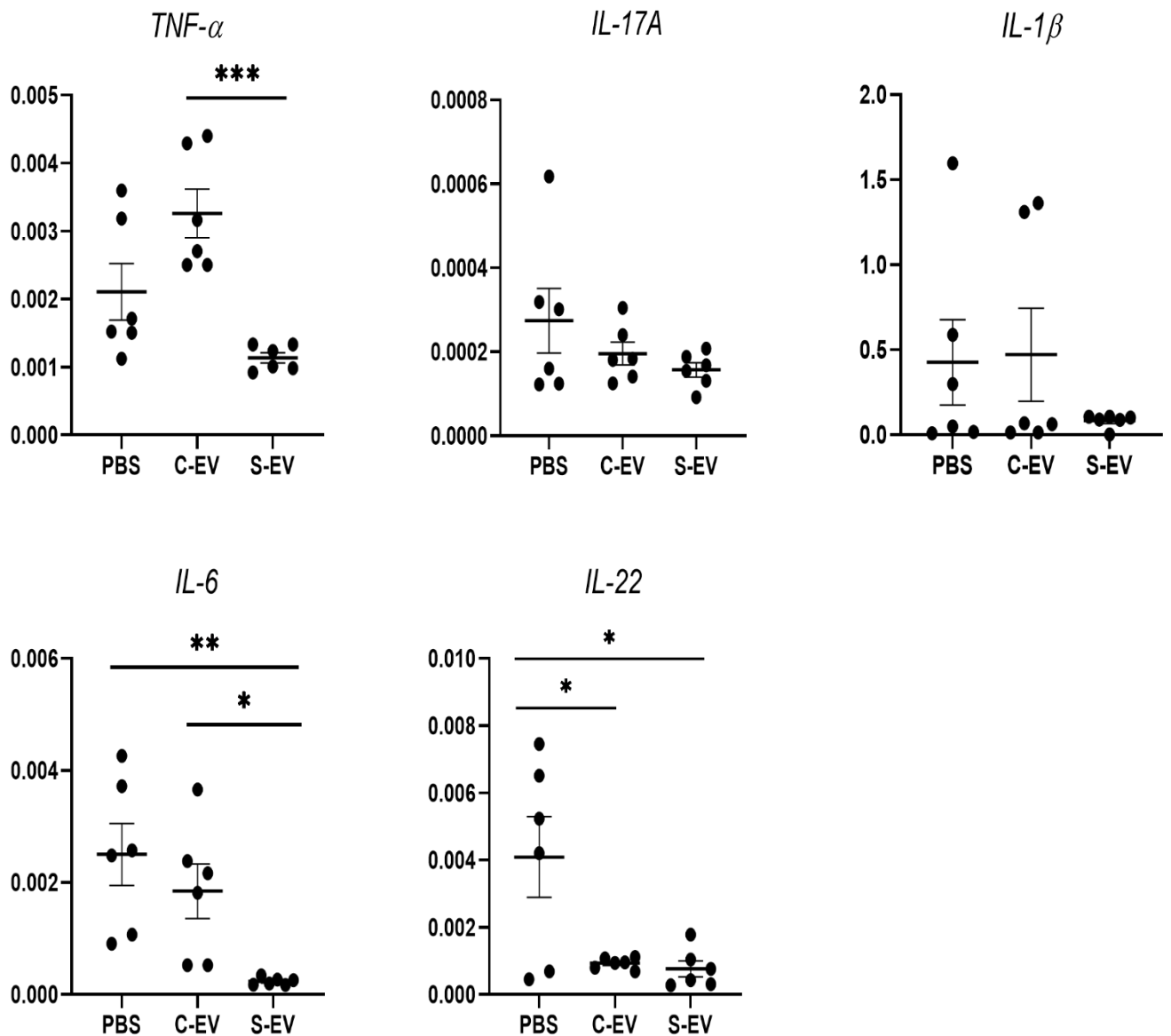


Figure S6. RT-qPCR analysis for gene expressions of *TNF-α*, *IL-17A*, *IL-1β*, *IL-6*, and *IL-22*. Relative expression of genes in ileal-loop tissues of the healthy mice treated with the EVs isolated by UC. PBS, phosphate-buffered saline (200 μ L); C-EV, control EVs (50 μ g/200 μ L) injected; S-EV, sepsis EVs (50 μ g/200 μ L) injected into ileal space. Other abbreviations: *TNF-α*, tumor necrosis factor- α ; IL, interleukin. N=6 mice per group. * p <0.05; ** p <0.01; and *** p <0.001.

Figure S7

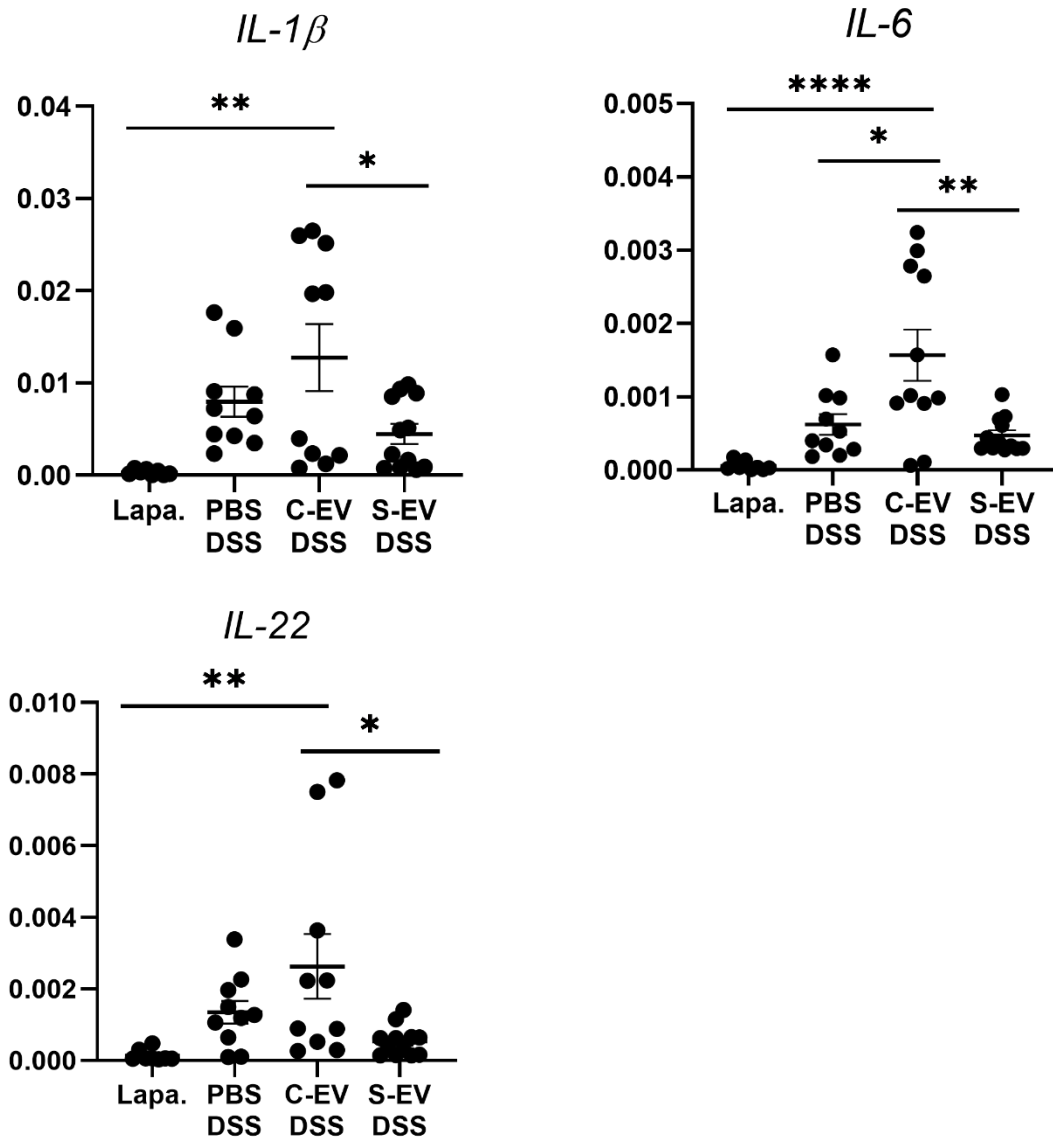


Figure S7. RT-qPCR analysis for gene expressions of *IL-1β*, *IL-6*, and *IL-22*. Relative expression of genes in ileal-loop tissues of the gut-inflamed mice treated with the EVs isolated by UC. Lapa, Laparotomy; PBS, phosphate-buffered saline (200 μ L); C-EV, control EVs (50 μ g/200 μ L) injected; S-EV, sepsis EVs (50 μ g/200 μ L) injected into ileal space. Other abbreviations: TNF- α , tumor necrosis factor- α ; IL, interleukin. N=8-12 mice per group. * p <0.05; ** p <0.01; and *** p <0.001.

Figure S8

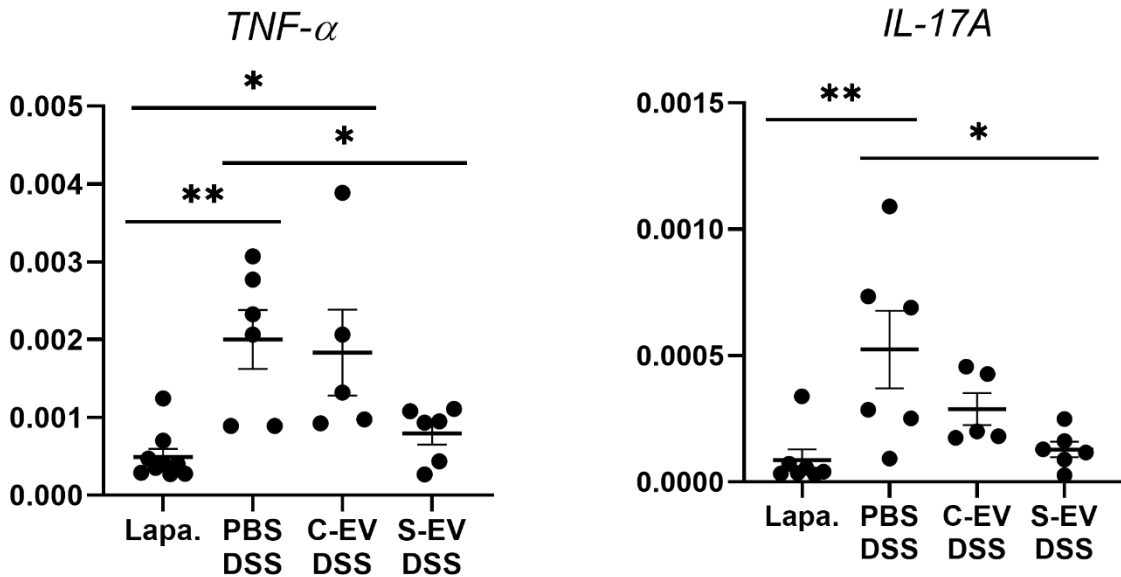


Figure S8. RT-qPCR analysis for gene expressions of *TNF- α* and *IL-17A*. Relative expression of genes in ileal-loop tissues of the gut-inflamed mice treated with the EVs isolated by C-DGUC. Lapa, Laparotomy; PBS, phosphate-buffered saline (200 μ L); C-EV, control EVs (50 μ g/200 μ L) injected; S-EV, sepsis EVs (50 μ g/200 μ L) injected into ileal space;. Other abbreviations: *TNF- α* , tumor necrosis factor- α ; *IL-17A*, interleukin-17A. N=5-8 mice per group. * p <0.05; and ** p <0.01.

Figure S9

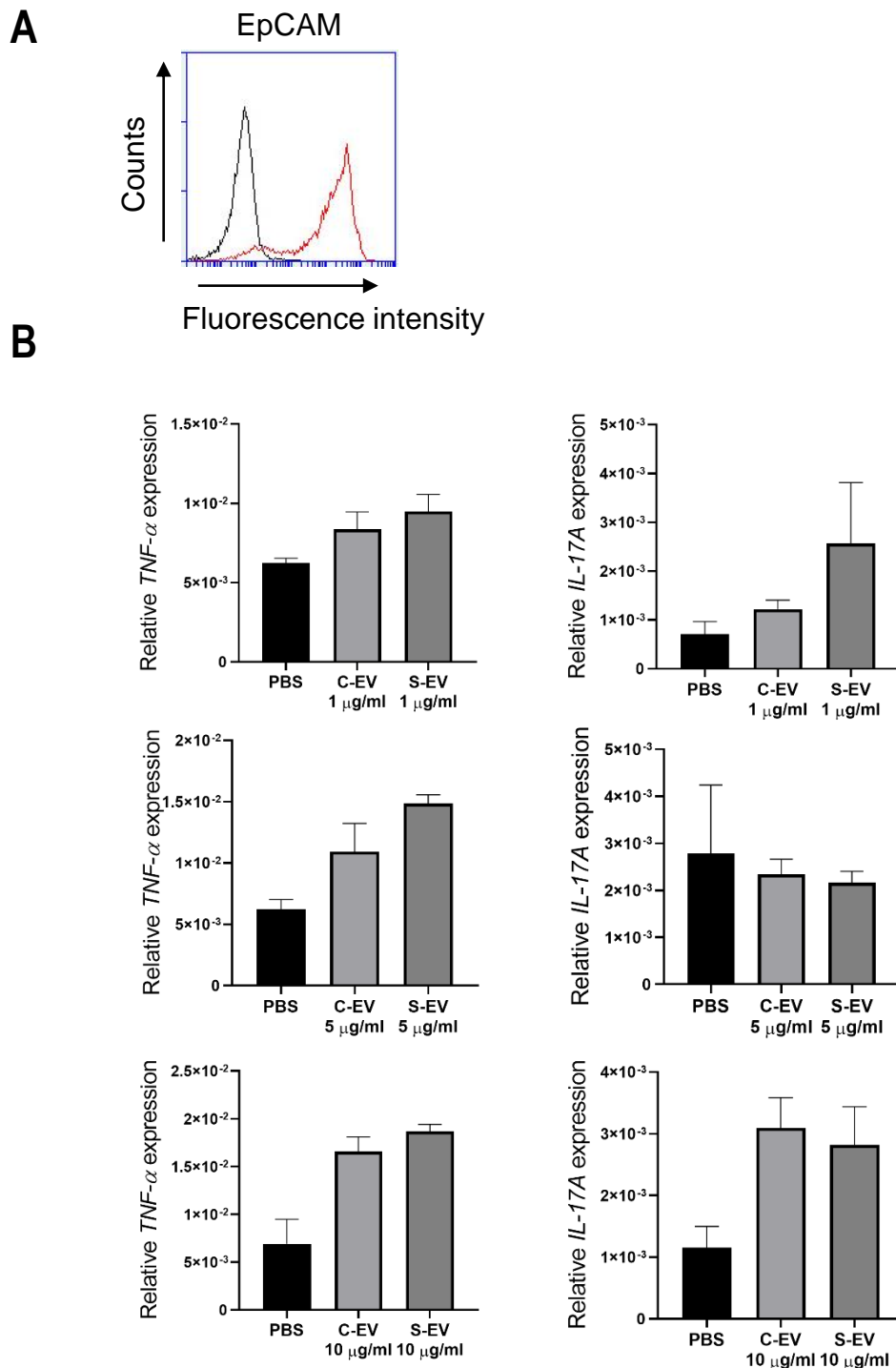
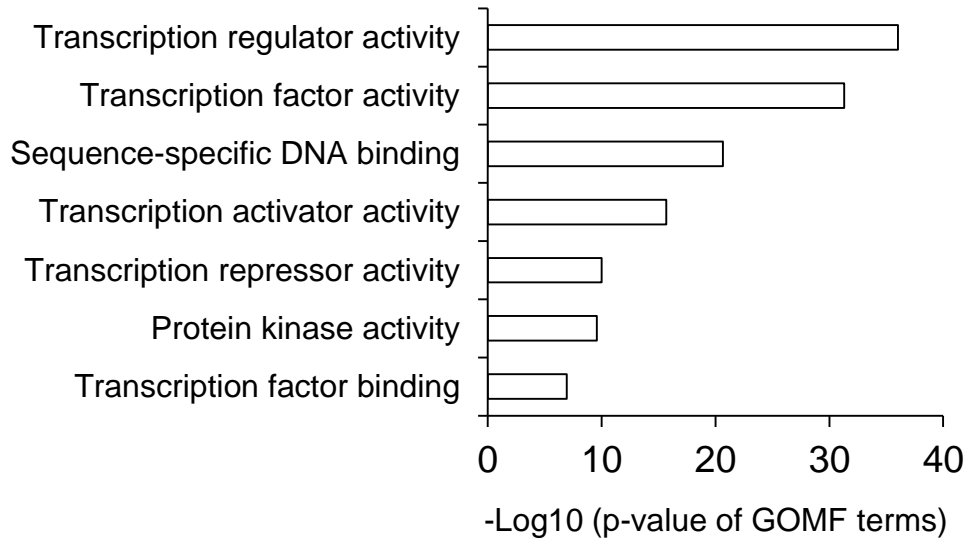


Figure S9. Confirmation of EpCAM expression and analysis of EV effects on altering *TNF- α* and *IL-17A* expressions in mouse IECs. (A) Representative histogram for analyzing EpCAM expression using flow cytometry. Black line, isotype control; and red line, anti-EpCAM MAb. (B) The IECs were treated with indicated doses of EVs for 24 hours and then subjected to RT-qPCR. Relative expression of both genes to *β -actin* was analyzed using $2^{-\Delta CT}$ method. 4 mice per group were used to isolate IECs and 3 to 4 independent experiments were conducted. Results are shown as the mean \pm SEM.

Figure S10

A



B

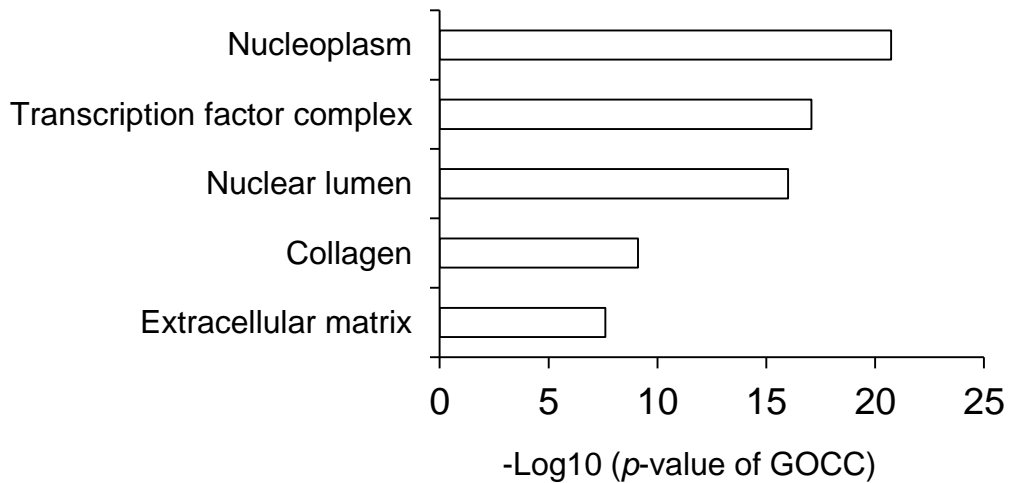


Figure S10. Gene Ontology (GO) enrichment analysis. (A) Gene Ontology Molecular Function (GOMF) terms enriched in target genes shared by upregulated microRNAs in septic EVs. (B) Gene Ontology Cellular Component (GOCC) terms enriched in target genes shared by upregulated microRNAs in septic EVs.

Table S1. Primer sequences used in RT-qPCR

	Forward (5' → 3')	Reverse (5' → 3')
TNF- α	ATAGCTCCCAGAAAAGCAAGC	CACCCCGAAGTTCAGTAGACA
IL-17A	TCTCCACCGCAATGAAGACC	CACACCCACCAGCATCTTCT
IL-1 β	GCCTTGGGCCTCAAAGGAAAGAATC	GGAAGACACAGATTCCATGGTGAAG
IL-6	TGGAGTCACAGAAGGAGTGGCTAAG	TCTGACCACAGTGAGGAATGTCCAC
IL-10	ATAACTGCACCCACTTCCCA	GGGCATCACTTCTACCAGGT
IL-22	TTGAGGTGTCCA ACTTCCAGCA	AGCCGGACGTCTGTGTTGTTA
CCL3	TGAAACCAGCAGCCTTTGCTC	AGGCATT CAGTTC CAGGTCAGTG
β -actin	CATCGTACTCCTGCTTGCTG	AGCGCAAGTACTCTGTGTGG
miR-19a	TGTGCAAATCTATGCAAACTGA	Universal primer
miR-21a	TAGCTTATCAGACTGATGTTGA	Universal primer
miR-22	AAGCTGCCAGTTGAAGAACTGT	Universal primer
miR-27a	TTCACAGTGGCTAAGTTCCGC	Universal primer
miR-103-2	AGCTTCTTTACAGTGCTGCCTTG	Universal primer
miR-107	AGCAGCATTGTACAGGGCTATCA	Universal primer
miR-126a	TCGTACCGTGAGTAATAATGCG	Universal primer
miR-146b	TGAGAACTGAATTCCATAGGCT	Universal primer
miR-182	TTTGGCAATGGTAGAACTCACACCG	Universal primer
miR-200b	TAATACTGCCTGGTAATGATGA	Universal primer
miR-203	GTGAAATGTTTAGGACCACTAG	Universal primer
miR-762	GGGGCTGGGGCCGGGACAGAGC	Universal primer
U6	GCGCGTCGTGAAGCGTTC	GTGCAGGGTCCGAGGT

Table S2. All miRNAs detected, RPKM values, and fold changes

miRNA	ENSEMBL No.	RPKM		Fold change (Sepsis/Control EV)
		Control EV	Sepsis EV	
Mir6236	ENSMUSG00000098973.1	439627	606258	1.379028131
Mir320	ENSMUSG00000065528.1	3538.031	49236.06	13.91623194
Mir6240	ENSMUSG00000098343.1	25941.69	37420	1.442465776
Mir6239	ENSMUSG00000098648.1	8929.15	18945.94	2.121807787
Mir21a	ENSMUSG00000065455.1	718.601	16479.41	22.93262882
Mir194-1	ENSMUST00000083647.1	2341.455	13078.69	5.585710594
Mir192	ENSMUSG00000065523.1	1360.412	10876.74	7.995180872
Mir200a	ENSMUST00000083466.1	225.1512	9292.76	41.27341982
Mir23a	ENSMUSG00000065611.1	212.0566	7130.2	33.62404188
Mir194-2	ENSMUSG00000065582.1	852.43	6371.319	7.474301702
Mir6538	ENSMUST00000183713.1	1926.7486	4714.477	2.446856326
Mir2137	ENSMUSG00000089357.1	1657.098	4630.18	2.794149773
Mir30d	ENSMUSG00000065437.1	447.204	4496.043	10.05367349
Mir200c	ENSMUSG00000065462.2	297.7676	3704.962	12.44246184
Mir205	ENSMUST00000083599.1	178.53	3678.86	20.60639668
Mir26a-2	ENSMUSG00000065430.1	450.714	3621.92	8.03596072
Mir200b	ENSMUST00000083615.2	210.9703	3569.403	16.91898338
Mir451a	ENSMUSG00000070065.1	2618.429	3531.736	1.348799605
Mir145a	ENSMUST00000083658.1	2828.588	3512.51	1.24178919
Mir10a	ENSMUSG00000065519.1	378.0462	3413.202	9.028531433
Mir215	ENSMUSG00000065562.1	511.3293	3355.749	6.56279427
Mir26a-1	ENSMUST00000083579.1	362.995	3071.744	8.462221243
Mirlet7b	ENSMUST00000083630.1	603.601	2684.378	4.447272287
Mir30c-2	ENSMUSG00000065567.1	304.91402	2565.767	8.414722944
Mir429	ENSMUST00000083493.1	317.0862	2523.109	7.957170637
Mir141	ENSMUST00000083540.1	0	2458.856	
Mir30b	ENSMUST00000083542.2	187.2548	2307.965	12.32526483
Mir375	ENSMUST00000083682.2	12.4285	2189.302	176.151748
Mir30c-1	ENSMUSG00000065490.1	260.80818	2186.087	8.381972529
Mir139	ENSMUST00000083512.1	22.4774	2174.319	96.73356349
Mir223	ENSMUST00000102112.1	5.8594	2167.223	369.8711472
Mir143	ENSMUST00000083511.2	2896.89	2113.505	0.729577236
Mir484	ENSMUST00000093566.1	87.2046	2097.76	24.05561175
Mir30a	ENSMUSG00000065405.2	287.4851	1958.073	6.811041685
Mir151	ENSMUSG00000065612.1	108.288	1933.113	17.8515902

Mir23b	ENSMUSG00000065599.1	448.565	1752.293	3.906441653
Mir29a	ENSMUST00000083676.1	49.3168	1529.198	31.00764851
Mir5100	ENSMUSG00000092734.1	88.5256	1356.4469	15.3226513
Mirlet7g	ENSMUSG00000065440.1	260.1841	1329.393	5.109432129
Mir203	ENSMUSG00000065574.1	110.6	1312.204	11.8644123
Mirlet7c-2	ENSMUST00000083674.1	518.882	1302.325	2.509867369
Mir5126	ENSMUST00000175513.1	863.767	1298.045	1.50277216
Mir10b	ENSMUST00000083566.2	177.355	1174.837	6.624211328
Mir5112	ENSMUSG00000092638.1	35.6625	1034.777	29.01582895
Mirlet7f-2	ENSMUST00000083668.1	343.147	965.111	2.812529324
Mir27a	ENSMUST00000083510.1	193.6441	893.084	4.611986629
Mir19b-2	ENSMUST00000083539.1	112.7751	868.212	7.698614322
Mirlet7c-1	ENSMUSG00000065557.2	361.155	861.361	2.385017513
Mir140	ENSMUSG00000065439.1	17.9234	816.772	45.57014852
Mir106b	ENSMUSG00000065514.1	106.358	810.65	7.621899622
Mir19b-1	ENSMUST00000102301.1	98.448	765.517	7.775851211
Mir425	ENSMUST00000083645.1	38.0733	712.9557	18.72587089
Mir1900	ENSMUSG00000084663.1	81.2055	702.4892	8.650758877
Mir183	ENSMUSG00000065619.2	0	682.8239	
Mir103-2	ENSMUST00000083629.1	196.22	682.289	3.477163388
Mir93	ENSMUSG00000065527.1	47.9814	678.321	14.13716565
Mir103-1	ENSMUSG00000065553.1	195.8214	671.496	3.429124702
Mir182	ENSMUSG00000076361.1	40.973	669.0016	16.32786469
Mir31	ENSMUSG00000065408.1	23.6661	639.6094	27.02639641
Mir1961	ENSMUSG00000089268.1	23.7726	637.2842	26.80750949
Mir16-2	ENSMUSG00000065606.1	141.0338	628.661	4.457520112
Mir30e	ENSMUSG00000065409.1	21.6168	546.2993	25.27197828
Mir92-1	ENSMUSG00000076062.1	14.3923	537.1531	37.32225565
Mirlet7a-2	ENSMUSG00000092770.1	182.3699	521.703	2.860685892
Mirlet7a-1	ENSMUSG00000065421.2	154.9924	503.108	3.246017224
Mirlet7d	ENSMUST00000083519.1	64.3387	500.797	7.783760008
Mir150	ENSMUSG00000065495.1	0	497.815	
Mir125b-2	ENSMUSG00000065472.1	237.436	490.2327	2.064694065
Mir24-2	ENSMUST00000083607.1	140.1455	479.182	3.419175072
Mir8114	ENSMUST00000183582.1	120.96965	468.613	3.873806364
Mir29b-1	ENSMUST00000083670.1	15.4662	443.759	28.69218037
Mir17	ENSMUST00000083574.1	112.8583	431.763	3.825708876
Mir125a	ENSMUSG00000065479.1	194.38578	418.9449	2.155224009
Mir29b-2	ENSMUSG00000065412.2	12.9301	393.742	30.45158197

Mir125b-1	ENSMUSG00000093354.1	189.378	390.169	2.060265712
Mir345	ENSMUST00000083495.1	79.01686	389.5542	4.930013671
Mir26b	ENSMUST00000083534.1	260.0754	384.545	1.47859044
Mir126a	ENSMUST00000083606.1	0	373.147	
Mir3068	ENSMUST00000083004.1	101.725	365.7393	3.595372819
Mir19a	ENSMUSG00000065416.1	0	362.564	
Mir27b	ENSMUST00000083541.1	0	346.4779	
Mir652	ENSMUSG00000076011.1	65.3752	322.9616	4.940124084
Mir20a	ENSMUSG00000065442.1	0	315.9133	
Mir22	ENSMUST00000083595.1	7.16726E-30	296.117	4.13152E+31
Mir146	ENSMUSG00000065601.1	0	286.1431	
Mir15a	ENSMUST00000175266.1	0.000169239	230.509	1362032.392
Mir3060	ENSMUSG00000093080.1	101.14	229.205	2.266215147
Mir18	ENSMUST00000083469.1	78.45823	228.5649	2.913204899
Mir802	ENSMUSG00000076457.1	0	215.7689	
Mir133a-1	ENSMUST00000083465.1	0	210.5098	
Mir148a	ENSMUSG00000065505.1	8.9672	207.86	23.1800339
Mir5099	ENSMUSG00000092998.1	0	204.7156	
Mir3100	ENSMUSG00000092659.1	150.386	203.6243	1.354011012
Mir3963	ENSMUSG00000092830.1	0	197.2544	
Mir423	ENSMUSG00000065518.2	6.88462	192.9491	28.02610747
Mir1247	ENSMUSG00000080356.1	154.3272	192.5977	1.247982857
Mir107	ENSMUSG00000065594.1	54.6206	190.3094	3.484205593
Mir1945	ENSMUSG00000088544.1	22.8779	186.596	8.15616818
Mir130a	ENSMUST00000083550.1	211.524	181.3982	0.857577391
Mir5117	ENSMUSG00000065160.1	0	179.3128	
Mir574	ENSMUSG00000077042.2	121.849	175.844	1.443130432
Mir186	ENSMUST00000083497.1	22.042	171.6925	7.789333999
Mir7672	ENSMUST00000184349.1	220.219	163.1352	0.740786217
Mir185	ENSMUSG00000065464.1	0	156.223	
Mir196b	ENSMUSG00000065443.1	19.6982	153.3961	7.787315592
Mir503	ENSMUST00000102168.1	0	144.8199	
Mir744	ENSMUST00000103261.1	0	144.7817	
Mir181a-2	ENSMUST00000083489.1	0	138.6642	
Mir717	ENSMUSG00000076214.1	514.7951	138.228	0.268510714
Mir5131	ENSMUST00000175426.1	146.8719	137.7874	0.93814678
Mir1983	ENSMUST00000157523.1	16.9478	136.172	8.034789176
Mir133a-2	ENSMUST00000083526.1	0	134.5549	
Mir147	ENSMUST00000102354.2	0	134.4315	

Mir29c	ENSMUSG00000065548.1	0	131.9434	
Mirlet7i	ENSMUST00000083472.2	23.1966	128.8228	5.553520775
Mir101a	ENSMUST00000083517.1	0	115.3006	
Mir7-2	ENSMUSG00000065609.1	33.6854	113.5778	3.371721874
Mir341	ENSMUSG00000070101.1	170.6122	113.3567	0.664411455
Mir181a-1	ENSMUST00000083631.1	0	112.3415	
Mir210	ENSMUSG00000065551.1	0	110.2281	
Mir378c	ENSMUST00000184478.1	0	107.8456	
Mir365-1	ENSMUST00000083515.1	45.2313	102.5945	2.268219131
Mir199a-1	ENSMUSG00000065547.1	7.718	100.355	13.00272091
Mir762	ENSMUSG00000076454.1	37.8262	99.9531	2.642430379
Mir122	ENSMUST00000083468.1	0	99.9227	
Mir33	ENSMUST00000083531.1	0	99.5146	
Mir342	ENSMUSG00000065436.1	73.7459	97.7418	1.325386225
Mir374b	ENSMUST00000102314.1	0	97.68393	
Mir144	ENSMUSG00000065401.1	0	88.7005	
Mir99a	ENSMUSG00000065530.1	104.23	85.7015	0.822234481
Mir7-1	ENSMUSG00000065434.1	24.9955	84.7354	3.390026205
Mir718	ENSMUSG00000076127.1	78.3628	82.8833	1.057686811
Mir1957a	ENSMUSG00000088552.1	27.1997	77.7339	2.857895491
Mir25	ENSMUSG00000065394.1	0	76.1275	
Mir361	ENSMUSG00000065510.1	0	75.2315	
Mir340	ENSMUSG00000065417.1	0	74.6328	
Mir1948	ENSMUSG00000087950.1	96.2838	73.9492	0.768033667
Mir7240	ENSMUSG00000099031.1	49.0631	72.8168	1.484145926
Mir674	ENSMUST00000102421.1	0	72.1656	
Mir98	ENSMUST00000083602.2	0	67.8007	
Mir193a	ENSMUST00000083461.1	0	66.5553	
Mir196a-1	ENSMUSG00000065546.1	2.75961	66.3291	24.03567895
Mir28a	ENSMUSG00000065494.1	0	66.0922	
Mir483	ENSMUSG00000070140.1	0	64.86761	
Mir872	ENSMUST00000104728.1	0	62.6605	
Mir21c	ENSMUSG00000099326.1	0	61.093	
Mir152	ENSMUST00000083581.1	0	60.9892	
Mir700	ENSMUST00000102169.1	4.32954	59.61031	13.76827792
Mir8109	ENSMUSG00000098388.1	30.6001	58.7669	1.920480652
Mir106a	ENSMUSG00000065456.1	0	57.9363	
Mir582	ENSMUST00000103758.2	42.85608	56.198	1.311319187
Mir187	ENSMUSG00000065532.1	0	55.4029	

Mir5709	ENSMUST00000176783.1	2.85611	54.6094	19.12020195
Mir130b	ENSMUSG00000065572.1	0	53.9914	
Mir1224	ENSMUSG00000080669.1	0	53.8164	
Mir145b	ENSMUSG00000098366.1	212.8334	53.1391	0.249674628
Mir196a-2	ENSMUSG00000065488.1	0	52.774	
Mir365-2	ENSMUST00000083555.1	22.9845	52.134	2.268224238
Mir96_	ENSMUSG00000065586.1	0	51.6659	
Mir3106	ENSMUST00000175401.1	343.55	51.0791	0.14868025
Mir92-2	ENSMUST00000083679.1	0	48.07866	
Mir99b	ENSMUST00000083462.1	0	47.1088	
Mir149	ENSMUSG00000065470.1	0	46.38507	
Mir20b	ENSMUST00000102087.1	0	45.5841	
Mir128-1	ENSMUST00000083586.1	0	45.23755	
Mir7075	ENSMUST00000184187.1	36.775788	43.3489	1.17873477
Mir877	ENSMUST00000104738.1	13.4901	42.9332	3.182570922
Mir1901	ENSMUSG00000084565.1	24.8797	42.8569	1.722564983
Mir136	ENSMUSG00000070129.1	0	42.5626	
Mir5106	ENSMUST00000174936.1	0	40.8126	
Mir6958	ENSMUSG00000098663.1	0	40.2843	
Mir133b	ENSMUSG00000065480.1	0	40.02365	
Mir434	ENSMUSG00000070133.1	0	39.13195	
Mir615	ENSMUST00000102056.1	45.2722	38.88904	0.859004864
Mir153	ENSMUSG00000065538.1	0	38.6359	
Mir6936	ENSMUSG00000098282.1	42.3006	38.5199	0.910623017
Mir199b	ENSMUSG00000092807.1	9.03561	37.6519	4.16705679
Mir15b	ENSMUSG00000065580.1	7.69686	37.1318	4.824278992
Mir7008	ENSMUSG00000098890.1	145.3824	36.59128	0.251689888
Mir1839	ENSMUST00000175366.1	33.2215	35.80242	1.077688244
Mir181b-1	ENSMUST00000083524.1	0	35.6269	
Mir301	ENSMUSG00000065589.1	16.7058	35.1968	2.10686109
Mir7654	ENSMUSG00000098917.1	7.5287	35.1494	4.668721031
mmu-mir-191	ENSMUSG00000103103.1	4.88461	34.48747	7.060434712
Mir7003	ENSMUSG00000099091.1	0	33.7996	
Mir221	ENSMUSG00000065422.1	0	32.6159	
Mir100	ENSMUSG00000093011.1	0	32.3572	
Mir412	ENSMUST00000083636.1	17.6188	31.238	1.772992485
Mir6933	ENSMUST00000184982.1	0	31.2323	
Mir362	ENSMUST00000093592.1	0	30.85722	
Mir199a-2	ENSMUSG00000070126.1	1.87665	30.7005	16.3592039

Mir339	ENSMUST00000083659.1	0	30.69531	
Mir128-2	ENSMUST00000083507.1	13.8653	30.57908	2.205439478
Mir101b	ENSMUSG00000065556.1	8.22029	29.558	3.59573689
Mir455	ENSMUST00000093594.1	0	29.25225	
Mir324	ENSMUST00000083600.1	0	28.8558	
Mir672	ENSMUST00000102331.1	0	28.3244	
Mir541	ENSMUST00000102097.1	0	28.20714	
Mir8102	ENSMUSG00000098919.1	38.71212	27.91912	0.721198426
Mir326	ENSMUST00000083637.1	0	27.43728	
Mir337	ENSMUSG00000065526.3	0	26.9399	
Mir148b	ENSMUSG00000065560.1	0	26.74135	
Mir181b-2	ENSMUST00000083644.1	0	26.73158	
Mir668	ENSMUST00000183620.1	6.68318	26.12231	3.908664737
Mir677	ENSMUSG00000093245.1	0	26.06787	
Mir7662	ENSMUST00000184761.1	1.70698	25.1882	14.75600183
Mir7040	ENSMUST00000184661.1	7.61529	24.9814	3.280426615
Mir3113	ENSMUSG00000093219.1	18.321	24.93174	1.360828557
Mir34a	ENSMUST00000083559.1	58.8817	23.56345	0.400182909
Mir328	ENSMUST00000093622.1	0	23.127	
Mir675	ENSMUSG00000076275.1	0	22.7237	
Mir7071	ENSMUST00000184847.1	60.0436	22.4751	0.374312999
Mir330	ENSMUST00000083609.1	0	22.09056	
Mir214	ENSMUSG00000065516.1	0	21.9718	
Mir190a	ENSMUST00000102424.1	0	21.7084	
Mir421	ENSMUST00000083575.2	0	21.5385	
Mir146b	ENSMUSG00000070127.2	0	21.29503	
Mir92b	ENSMUST00000102300.2	0	21.1522	
Mir3473d	ENSMUST00000175346.1	0	20.9582	
Mir7648	ENSMUST00000183650.1	0	20.544	
Mir222	ENSMUST00000083537.1	0	20.18761	
Mir1932	ENSMUSG00000088015.1	22.0367	20.058	0.910208879
Mir486	ENSMUSG00000070084.3	3.78775	19.2763	5.08911623
Mir758	ENSMUST00000103260.1	0	18.84647	
Mir224	ENSMUSG00000065542.1	3.59529	18.2243	5.068937415
Mir181c	ENSMUSG00000065483.1	1.24558	17.4863	14.03868078
Mir1897	ENSMUSG00000084530.2	21.79756	16.84071	0.772596107
Mir212	ENSMUST00000083656.1	16.0107	16.57673	1.035353233
Mir490	ENSMUSG00000070075.1	0	16.5689	
Mir7235	ENSMUST00000183796.1	0	16.0079	

Mir3569	ENSMUSG00000098553.1	22.8961	15.943	0.696319461
Mir5625	ENSMUSG00000093710.1	37.8087	15.8649	0.419609772
Mir500	ENSMUSG00000070108.2	0	15.85214	
Mir7076	ENSMUSG00000099129.1	0	15.8361685	
Mir669a-11	ENSMUST00000179742.1	0	15.1306	
Mir598	ENSMUST00000102094.3	23.7658	15.0182	0.631924867
Mir6918	ENSMUSG00000098296.1	0	14.8119	
Mir501	ENSMUST00000102296.1	459.5762	14.53529	0.031627595
Mir693	ENSMUST00000102187.1	0	14.033524	
Mir1960	ENSMUSG00000088113.1	0	13.6301	
Mir3096	ENSMUST00000116685.1	0	13.586	
Mir369	ENSMUST00000083627.2	4.39962	13.3836	3.04198999
Mir3077	ENSMUSG00000092784.1	4.13509	13.25448	3.205366751
Mir379	ENSMUSG00000065498.3	0	13.024	
Mir219a-1	ENSMUSG00000065555.1	0.000166892	12.934877	77504.47595
Mir195a	ENSMUSG00000065411.2	104.2532	12.5854	0.120719556
Mir411	ENSMUSG00000065477.2	0	12.54403	
Mir7211	ENSMUST00000184071.1	0	12.4968	
Mir298	ENSMUSG00000065410.1	0	12.1373	
Mir3547	ENSMUSG00000093202.2	0	12.12809	
Mir6959	ENSMUST00000184827.1	0	12.121298	
Mir6984	ENSMUST00000185105.1	0	12.0134	
Mir532	ENSMUSG00000070139.1	0	11.5761	
Mir127	ENSMUSG00000070076.1	0	11.5635	
Mir331	ENSMUSG00000065607.1	0	11.428	
Mir8101	ENSMUSG00000098863.1	116.8116	11.426285	0.097818068
Mir671	ENSMUSG00000076387.1	11.8732	11.370882	0.957693124
Mir154	ENSMUST00000083514.1	99.4588	11.3568	0.114185974
Mir3104	ENSMUSG00000092652.1	0	11.3046	
Mir5122	ENSMUSG00000092745.1	2.12116	11.1551	5.258962077
Mir335	ENSMUST00000083567.1	0	11.12344	
Mir467d	ENSMUST00000103833.2	0	10.9618	
Mir5130	ENSMUST00000175160.1	1.75813E-36	10.901995	6.2009E+36
Mir291b	ENSMUSG00000078032.1	16.5668	10.76067	0.649532197
Mir7046	ENSMUSG00000098802.1	0	10.5443	
Mir1199	ENSMUST00000117015.1	6.1964E-102	10.3965	1.6778E+102
Mir1968	ENSMUST00000157429.1	0	10.1329	
Mir188	ENSMUSG00000065398.1	0	10.0887	
Mir378b	ENSMUSG00000092985.1	0	9.98646	

Mir7019	ENSMUST00000183998.1	3.35473	9.48575	2.827574797
Mir300	ENSMUST00000083485.2	0	9.43908	
Mir32	ENSMUSG00000065544.1	0	9.35358	
Mir8112	ENSMUSG00000098623.1	0	9.07021	
Mir6406	ENSMUSG00000099174.1	5.401	8.76736	1.623284577
Mir7013	ENSMUSG00000099033.1	0	8.6657	
Mir6921	ENSMUSG00000098547.1	0	8.42672	
Mir206	ENSMUST00000083625.1	19.8416	8.34547	0.420604689
Mir382	ENSMUSG00000065428.3	113.742	8.11414	0.071338116
Mir450b	ENSMUSG00000076050.1	0	8.1134	
Mir6979	ENSMUSG00000098706.1	0	8.09599	
Mir329	ENSMUST00000083643.1	0	7.70899	
Mir6349	ENSMUSG00000098833.1	0	7.68822	
Mir1193	ENSMUSG00000080411.1	2.64333	7.52933	2.848426038
Mir5132	ENSMUSG00000092907.1	0	7.29308	
Mir666	ENSMUSG00000076272.1	0	7.27816	
Mir350	ENSMUSG00000065573.1	0	7.14076	
Mir137	ENSMUST00000083635.1	0.000783821	7.01463	8949.275409
Mir135a-1	ENSMUSG00000065407.1	80.9461	6.89443	0.085173097
Mir467a-3	ENSMUST00000178082.1	0	6.79213	
Mir495	ENSMUSG00000070105.2	0	6.51201	
Mir6377	ENSMUSG00000098401.1	0	6.48323	
Mir1306	ENSMUST00000116802.2	0	6.22477	
Mir487b	ENSMUST00000102265.1	0	6.08505	
Mir1934	ENSMUST00000158127.1	0	5.88617	
Mir18b	ENSMUST00000103923.2	0	5.88617	
Mir467a-9	ENSMUSG00000095222.1	0	5.80197	
Mir34b	ENSMUST00000083558.1	0	5.69628	
Mir540	ENSMUSG00000072900.1	0	5.69628	
Mir378d	ENSMUSG00000098756.1	0	5.51512	
Mir6238	ENSMUSG00000099176.1	0	5.4807	
Mir1981	ENSMUSG00000088559.1	12.6001	5.44983	0.432522758
Mir7b	ENSMUST00000083557.1	0	5.37088	
Mir3102	ENSMUST00000175555.1	0	5.31024	
Mir7070	ENSMUSG00000099076.1	0	5.26132	
Mir3474	ENSMUSG00000093120.1	0	5.07227	
Mir1249	ENSMUST00000116791.1	0	5.06969	
Mir381	ENSMUST00000083632.2	0	4.71954	
Mir1964	ENSMUST00000158514.1	0	4.66675	

Mir5108	ENSMUSG00000093017.1	4.5176	4.59573	1.017294581
Mir431	ENSMUSG00000070080.1	0	4.5801	
Mir505	ENSMUST00000093573.2	0	4.57816	
Mir676	ENSMUST00000102443.1	0	4.53657	
Mir449a	ENSMUST00000083641.1	0	4.48385	
Mir297a-2	ENSMUSG00000076983.2	0	4.41161	
Mir8120	ENSMUST00000185035.1	0	4.40676	
Mir132	ENSMUST00000083603.1	0	4.26584228	
Mir129-1	ENSMUST00000083535.1	0	4.19261	
Mir5623	ENSMUST00000176631.1	0	4.14447	
Mir322	ENSMUSG00000065418.1	20.0384	4.07699	0.203458859
Mir7011	ENSMUSG00000098655.1	0	4.04498	
Mir432	ENSMUSG00000087855.1	0	3.89028	
Mir466d	ENSMUSG00000078031.1	0	3.7106	
Mir138-1	ENSMUST00000083480.1	0	3.64399	
Mir5119	ENSMUST00000175435.1	0	3.57603	
Mir669a-1	ENSMUSG00000096583.1	0	3.56708	
Mir669a-6	ENSMUST00000102064.1	0	3.56708	
Mir8097	ENSMUST00000185150.1	47.42631	3.562015	0.075106307
Mir3968	ENSMUST00000175355.1	4.97064	3.55195	0.714586049
Mir124a-3	ENSMUST00000083520.1	30.1542	3.45043	0.114426183
Mir7045	ENSMUSG00000098762.1	0.911637	3.42507	3.757054617
Mir6356	ENSMUSG00000099300.1	0	3.3688	
Mir6943	ENSMUSG00000099058.1	0	3.35298	
Mir134	ENSMUSG00000065426.2	0	3.33856	
Mir6370	ENSMUSG00000099149.1	0	3.29664	
Mir184	ENSMUST00000083662.1	4.01674	3.26896	0.813834104
Mir138-2	ENSMUSG00000065512.2	16.0033	3.25601	0.203458662
Mir8098	ENSMUSG00000099245.1	11.3642	3.19483	0.281131096
Mir7677	ENSMUST00000184226.1	5.50993	3.192237	0.579360718
Mir760	ENSMUSG00000076456.1	0	3.141688	
Mir7027	ENSMUSG00000098731.1	19.3915	3.11573	0.160675038
Mir8104	ENSMUST00000185165.1	7.91254E-07	3.04727	3851190.642
Mir6952	ENSMUSG00000098451.1	0	2.9872	
Mir338	ENSMUSG00000065600.1	0	2.90216	
Mir99ahg	ENSMUST00000182398.3	5.17424	2.883777	0.557333444
Mir5134	ENSMUSG00000093270.1	0	2.87644	
Mir142hg	ENSMUSG00000084796.1	0.238752	2.84264	11.90624581
Mir217	ENSMUSG00000065415.1	0	2.79764	

Mir1949	ENSMUSG00000088059.1	0	2.77865	
Mir680-2	ENSMUSG00000076117.1	0	2.75013	
Mir323	ENSMUST00000083683.1	99.92444	2.67074	0.026727595
Mir218-1	ENSMUSG00000065603.1	1.0671	2.66604	2.498397526
Mir3473e	ENSMUST00000183932.1	0	2.49247	
Mir218-2	ENSMUSG00000065583.1	1.51187	2.48444	1.643289436
Mir8105	ENSMUSG00000098957.1	2.98897	2.43252	0.81383219
Mir129-2	ENSMUSG00000065511.1	0	2.35977	
Mir6244	ENSMUSG00000099311.1	12.9755	2.34033	0.180365304
Mir6916	ENSMUSG00000099292.1	0	2.30376	
Mir7666	ENSMUST00000183849.1	0	2.11558	
Mir1938	ENSMUSG00000089371.1	61.9531	2.04891	0.033071953
Mir7060	ENSMUSG00000098267.1	0	1.9121	
Mir1191	ENSMUSG00000080533.1	0	1.74251	
Mir3076	ENSMUSG00000093156.1	0	1.70507	
Mir124a-2	ENSMUSG00000093073.1	16.3536	1.63152	0.099765189
Mir6417	ENSMUSG00000098726.1	5.89705	1.59543	0.270547138
Mir3109	ENSMUSG00000093042.1	0	1.48719	
Mir124-2hg	ENSMUST00000186923.1	0.00015064	1.452937	9645.094264
Mir6981	ENSMUSG00000098608.1	0	1.43695	
Mir702	ENSMUST00000102285.1	2.11236	1.31251	0.621347687
Mir299b	ENSMUSG00000093291.1	0	1.17333	
Mir6941	ENSMUST00000184711.1	2.19302	1.15342	0.525950516
Mir8111	ENSMUSG00000098823.1	0	1.04477	
Mir5110	ENSMUST00000175537.1	0	1.03513	
Mir1947	ENSMUSG00000088860.1	15.7143	0.989288	0.062954634
Mir7068	ENSMUSG00000099079.1	4.7437	0.897642	0.18922824
Mir3074-1	ENSMUSG00000092741.1	5.76691	0.782218	0.135639016
Mir22hg	ENSMUST00000134345.1	2.17207	0.51152	0.235498856
Mir124-2hg	ENSMUST00000189754.1	1.08238	0.24572323	0.227021219
Mir124-2hg	ENSMUST00000189467.1	3.70091	0.209082	0.056494754
Mir124a-1	ENSMUST00000083663.1	30.7759	0.00040736	1.32362E-05
Mir1896	ENSMUST00000122641.1	18.8082	0.00011116	5.90992E-06
Mir99ahg	ENSMUST00000182548.1	2.016994	8.8581E-07	4.39171E-07
Mir6944	ENSMUST00000182548.1	86.5956	0	0
Mir7044	ENSMUSG00000098583.1	63.6571	0	0
Mir7223	ENSMUST00000183433.1	54.9027	0	0
Mir494	ENSMUSG00000070141.2	54.2112	0	0
Mir7671	ENSMUSG00000099153.1	39.2505	0	0

Mir7007	ENSMUST00000184606.1	26.6807	0	0
Mir6368	ENSMUSG00000099158.1	19.9119	0	0
Mir878	ENSMUST00000104680.1	17.1584	0	0
Mir8092	ENSMUSG00000099118.1	16.7424	0	0
Mir707	ENSMUSG00000076051.1	15.8084	0	0
Mir1231	ENSMUST00000175639.1	15.0984	0	0
Mir6414	ENSMUSG00000098264.1	14.954	0	0
Mir292	ENSMUSG00000078041.1	14.954	0	0
Mir204	ENSMUSG00000065507.2	12.485	0	0
Mir6996	ENSMUSG00000098548.1	11.694	0	0
Mir7058	ENSMUST00000184637.1	9.9898	0	0
Mir7236	ENSMUST00000184435.1	9.1429	0	0
Mir688	ENSMUSG00000076009.1	8.86544	0	0
Mir6385	ENSMUSG00000098886.1	7.66388	0	0
Mir3062	ENSMUST00000174986.1	7.57894	0	0
Mir6937	ENSMUSG00000098579.1	5.47507	0	0
Mir1197	ENSMUST00000117037.1	5.401	0	0
Mir7023	ENSMUST00000185093.1	5.0642	0	0
Mir1905	ENSMUST00000122779.1	4.98467	0	0
Mir3086	ENSMUSG00000092813.1	4.23972	0	0
Mir7016	ENSMUSG00000098422.1	3.80327	0	0
Mir7001	ENSMUSG00000099238.1	3.68065	0	0
Mir7039	ENSMUSG00000098822.1	3.12336	0	0
Mir142hg	ENSMUST00000123700.1	2.82696	0	0
Mir433	ENSMUSG00000070072.1	2.48227	0	0
Mir207	ENSMUSG00000065452.1	2.39072	0	0
Mir6335	ENSMUSG00000098734.1	2.33053	0	0
Mir6241	ENSMUST00000184225.1	2.17795	0	0
Mir6350	ENSMUSG00000098876.1	1.91597	0	0
Mir6392	ENSMUST00000184924.1	1.46402	0	0
Mir99ahg	ENSMUST00000182986.1	1.20409	0	0

Table S3. RPKM values and fold change of miRNAs targeting TNF- α and IL-17A

miRNA	ENSEMBL No.	TNF- α			IL-17A		
		RPKM		Fold change (Sepsis/ Control EV)	RPKM		Fold change (Sepsis/ Control EV)
		Control EV	Sepsis EV		Control EV	Sepsis EV	
Mir320	ENSMUSG00000065528.1				3538.031	49236.06	13.916232
Mir6240	ENSMUSG00000098343.1				25941.69	37420	1.4424658
Mir21a	ENSMUSG00000065455.1				718.601	16479.41	22.932629
Mir200a	ENSMUST00000083466.1				225.1512	9292.76	41.27342
Mir200c	ENSMUSG00000065462.2				297.7676	3704.962	12.442462
Mir26a-2	ENSMUSG00000065430.1				450.714	3621.92	8.0359607
Mir200b	ENSMUST00000083615.2				210.9703	3569.403	16.918983
Mir429	ENSMUST00000083493.1				317.0862	2523.109	7.9571706
Mir30b	ENSMUST00000083542.2				187.2548	2307.965	12.325265
Mir203	ENSMUSG00000065574.1				110.6	1312.204	11.864412
Mir10b	ENSMUST00000083566.2				177.355	1174.837	6.6242113
Mir5112	ENSMUSG00000092638.1	35.6625	1034.777	29.015829	35.6625	1034.777	29.015829
Mir27a	ENSMUST00000083510.1	193.6441	893.084	4.6119866			
Mir140	ENSMUSG00000065439.1				17.9234	816.772	45.570149
Mir183	ENSMUSG00000065619.2				0	682.8239	
Mir103-2	ENSMUST00000083629.1				196.22	682.289	3.4771634
Mir103-1	ENSMUSG00000065553.1				195.8214	671.496	3.4291247
Mir182	ENSMUSG00000076361.1				40.973	669.0016	16.327865
Mir125a	ENSMUSG00000065479.1	194.38578	418.9449	2.155224			
Mir29b-2	ENSMUSG00000065412.2				12.9301	393.742	30.451582
Mir26b	ENSMUST00000083534.1				260.0754	384.545	1.4785904
Mir126a	ENSMUST00000083606.1				0	373.147	
Mir3068	ENSMUST00000083004.1	101.725	365.7393	3.5953728	101.725	365.7393	3.5953728
Mir19a	ENSMUSG00000065416.1	0	362.564		0	362.564	
Mir27b	ENSMUST00000083541.1	0	346.4779				
Mir22	ENSMUST00000083595.1				0	296.117	
Mir146a	ENSMUSG00000065601.1	0	286.1431				
Mir3060	ENSMUSG00000093080.1				101.14	229.205	2.2662151
Mir107	ENSMUSG00000065594.1				54.6206	190.3094	3.4842056
Mir130a	ENSMUST00000083550.1	211.524	181.3982	0.8575774			
Mir185	ENSMUSG00000065464.1	0	156.223		0	156.223	

Mir196b	ENSMUSG00000065443.1	19.6982	153.3961	7.7873156	19.6982	153.3961	7.7873156
Mir101a	ENSMUST00000083517.1	0	115.3006		0	115.3006	
Mir210	ENSMUSG00000065551.1				0	110.2281	
Mir762	ENSMUSG00000076454.1	37.8262	99.9531	2.6424304			
Mir33	ENSMUST00000083531.1	0	99.5146				
Mir99a	ENSMUSG00000065530.1	104.23	85.7015	0.8222345	104.23	85.7015	0.8222345
Mir25	ENSMUSG00000065394.1	0	76.1275		0	76.1275	
Mir674	ENSMUST00000102421.1	0	72.1656				
Mir582	ENSMUST00000103758.2	42.85608	56.198	1.3113192	42.85608	56.198	1.3113192
Mir130b	ENSMUSG00000065572.1	0	53.9914		0	53.9914	
Mir96	ENSMUSG00000065586.1				0	51.6659	
Mir3106	ENSMUST00000175401.1				343.55	51.0791	0.1486803
Mir99b	ENSMUST00000083462.1	0	47.1088		0	47.1088	
Mir149	ENSMUSG00000065470.1	0	46.38507		0	46.38507	
Mir7075	ENSMUST00000184187.1	36.775788	43.3489	1.1787348			
Mir877	ENSMUST00000104738.1				13.4901	42.9332	3.1825709
Mir133b	ENSMUSG00000065480.1	0	40.02365				
Mir6936	ENSMUSG00000098282.1	42.3006	38.5199	0.910623			
Mir199b	ENSMUSG00000092807.1	9.03561	37.6519	4.1670568			
Mir1839	ENSMUST00000175366.1	33.2215	35.80242	1.0776882	33.2215	35.80242	1.0776882
Mir301a	ENSMUSG00000065589.1	16.7058	35.1968	2.1068611			
Mir7003	ENSMUSG00000099091.1	0	33.7996				
Mir100	ENSMUSG00000093011.1	0	32.3572				
Mir412	ENSMUST00000083636.1				17.6188	31.238	1.7729925
Mir101b	ENSMUSG00000065556.1	8.22029	29.558	3.5957369	8.22029	29.558	3.5957369
Mir455	ENSMUST00000093594.1	0	29.25225				
Mir326	ENSMUST00000083637.1				0	27.43728	
Mir337	ENSMUSG00000065526.3	0	26.9399				
Mir677	ENSMUSG00000093245.1	0	26.06787				
Mir7662	ENSMUST00000184761.1				1.70698	25.1882	14.756002
Mir328	ENSMUST00000093622.1	0	23.127		0	23.127	
Mir330	ENSMUST00000083609.1				0	22.09056	
Mir421	ENSMUST00000083575.2				0	21.5385	
Mir146b	ENSMUSG00000070127.2				0	21.29503	
Mir92b	ENSMUST00000102300.2	0	21.1522		0	21.1522	
Mir7648	ENSMUST00000183650.1	0	20.544				
Mir181c	ENSMUSG00000065483.1	1.24558	17.4863	14.038681			

Mir5625	ENSMUSG00000093710.1				37.8087	15.8649	0.4196098
Mir7076	ENSMUSG00000099129.1	0	15.836168				
Mir6918	ENSMUSG00000098296.1				0	14.8119	
Mir3096	ENSMUST00000116685.1	0	13.586				
Mir411	ENSMUSG00000065477.2	0	12.54403				
Mir298	ENSMUSG00000065410.1	0	12.1373				
Mir3547	ENSMUSG00000093202.2	0	12.12809				
Mir6959	ENSMUST00000184827.1	0	12.121298				
Mir6984	ENSMUST00000185105.1				0	12.0134	
Mir154	ENSMUST00000083514.1				99.4588	11.3568	0.114186
Mir335	ENSMUST00000083567.1				0	11.12344	
Mir467d	ENSMUST00000103833.2	0	10.9618				
Mir291b	ENSMUSG00000078032.1	16.5668	10.76067	0.6495322			
Mir1199	ENSMUST00000117015.1	0	10.3965		0	10.3965	
Mir188	ENSMUSG00000065398.1	0	10.0887				
Mir300	ENSMUST00000083485.2				0	9.43908	
Mir32	ENSMUSG00000065544.1	0	9.35358		0	9.35358	
Mir450b	ENSMUSG00000076050.1	0	8.1134		0	8.1134	
Mir1193	ENSMUSG00000080411.1	2.64333	7.52933	2.848426			
Mir5132	ENSMUSG00000092907.1	0	7.29308		0	7.29308	
Mir350	ENSMUSG00000065573.1	0	7.14076				
Mir137	ENSMUST00000083635.1				0	7.01463	
Mir495	ENSMUSG00000070105.2				0	6.51201	
Mir1934	ENSMUST00000158127.1				0	5.88617	
Mir540	ENSMUSG00000072900.1	0	5.69628				
Mir1981	ENSMUSG00000088559.1				12.6001	5.44983	0.4325228
Mir3102	ENSMUST00000175555.1	0	5.31024				
Mir1249	ENSMUST00000116791.1				0	5.06969	
Mir3968	ENSMUST00000175355.1				4.97064	3.55195	0.714586
Mir6370	ENSMUSG00000099149.1	0	3.29664				
Mir184	ENSMUST00000083662.1	4.01674	3.26896	0.8138341			
Mir760	ENSMUSG00000076456.1	0	3.141688				
Mir7027	ENSMUSG00000098731.1	19.3915	3.11573	0.160675			
Mir338	ENSMUSG00000065600.1	0	2.90216				
Mir323	ENSMUST00000083683.1	99.92444	2.67074	0.0267276			
Mir3076	ENSMUSG00000093156.1				0	1.70507	
Mir3109	ENSMUSG00000093042.1	0	1.48719		0	1.48719	

Mir6981	ENSMUSG00000098608.1	0	1.43695	0	1.43695		
Mir5110	ENSMUST00000175537.1	0	1.03513				
Mir7068	ENSMUSG00000099079.1				4.7437	0.897642	0.1892282
Mir3074-1	ENSMUSG00000092741.1				5.76691	0.782218	0.135639
Mir292a	ENSMUSG00000078041.1	14.954	0	0			
Mir204	ENSMUSG00000065507.2	12.485	0	0	12.485	0	0
Mir7016	ENSMUSG00000098422.1				3.80327	0	0
Mir7058	ENSMUST00000184637.1	9.9898	0	0			
Mir7236	ENSMUST00000184435.1	9.1429	0	0			
Mir3062	ENSMUST00000174986.1	7.57894	0	0			
Mir1197	ENSMUST00000117037.1	5.401	0	0			
Mir7039	ENSMUSG00000098822.1				3.12336	0	0